

MICROCOPY RESOLUTION TEST CHART

NATIONAL BUREAU OF STANDARDS-1963-A

LEVEL III

AP-E 300752

B.S. 12

✓ DNA 4800F

ANA 084655

ANALYSIS OF ENERGY-ABSORBING FOUNDATIONS

Department of Engineering Science and Mechanics
The Pennsylvania State University
University Park, Pennsylvania 16802

15 December 1978

Final Report for Period 1 December 1977-15 December 1978

CONTRACT No. DNA 001-78-C-0036

APPROVED FOR PUBLIC RELEASE;
DISTRIBUTION UNLIMITED.

62-12-78

THIS WORK SPONSORED BY THE DEFENSE NUCLEAR AGENCY
UNDER RDT&E RMSS CODE B344078464 Y99QAXSF50311 H2590D.

S DTIC ELECTE **D**
MAY 23 1980
D

FILE COPY

Prepared for
Director
DEFENSE NUCLEAR AGENCY
Washington, D. C. 20305

Destroy this report when it is no longer
needed. Do not return to sender.

PLEASE NOTIFY THE DEFENSE NUCLEAR AGENCY,
ATTN: STTI, WASHINGTON, D.C. 20305, IF
YOUR ADDRESS IS INCORRECT, IF YOU WISH TO
BE DELETED FROM THE DISTRIBUTION LIST, OR
IF THE ADDRESSEE IS NO LONGER EMPLOYED BY
YOUR ORGANIZATION.



UNCLASSIFIED

SECURITY CLASSIFICATION OF THIS PAGE(When Data Entered)

20. ABSTRACT (Continued)

Quasistatic tests were performed for honeycomb, axially and side-loaded tubes, and clamped-clamped beams, all for large deformations. Intermediate rate tests and shock-machine tests were performed of honeycomb, side-loaded tubes, and clamped-clamped beams. Analytical procedures were developed to predict the response of side-loaded tubes and beams, based on finite difference and finite element techniques.

| | |
|--------------------|-------------------------------------|
| Accession For | |
| NTIS GRA&I | <input checked="" type="checkbox"/> |
| DDC TAB | <input type="checkbox"/> |
| Unannounced | <input type="checkbox"/> |
| Justification | |
| By _____ | |
| Distribution/ | |
| Availability Codes | |
| Dist. | Avail and/or special |
| A | |

DTIC
ELECTE
MAY 23 1980
S D D

UNCLASSIFIED

SECURITY CLASSIFICATION OF THIS PAGE(When Data Entered)

PREFACE

This report summarizes results of a one year study dealing with the development of analytical methods for predicting response of energy-absorbing foundations on ships undergoing nuclear weapons attack. In the first phase of the study, a survey was made of the literature dealing with various energy-absorbing configurations and the associated dynamic material behavior. In the second phase, study was begun of configurations that showed promise for use in ships, namely side-loaded tubes, axially loaded tubes, honeycomb, and beams. Tests were conducted in conventional test machines at various rates and in a drop-table shock machine. Analytical methods were developed for side-loaded tubes and beams.

This work was sponsored by the Defense Nuclear Agency under RDT&E RMSS Code B3440 78464 Y99QAXSF503-11 H2590D.

The benefit of technical discussions with Lt. R. Wade, Lt. R. Elsbernd, and Dr. Nicholas Perrone is gratefully acknowledged. The computer analysis of the simulated machine-foundation configuration under shock machine loading was performed by Mr. Koorosh Kasraie, graduate student in the Department of Engineering Science and Mechanics at The Pennsylvania State University.

Table 1. Conversion factors for U. S. customary to metric (SI) units of measurement.

| To Convert From | To | Multiply by |
|---|--|-----------------|
| foot | meter (m) | 3.048000 X E -1 |
| foot-pound-force | joule (J) | 1.355818 |
| inch | meter (m) | 2.540000 X E -2 |
| kip (1000 lbf) | newton (N) | 4.448222 X E +3 |
| kip/inch ² (ksi) | kilo pascal (kPa) | 6.894757 X E +3 |
| pound-force | newton (N) | 4.448222 |
| pound-force inch | newton-meter (N•m) | 1.129848 X E -1 |
| pound-force/inch | newton/meter (N/m) | 1.751268 X E +2 |
| pound-force/foot ² | kilo pascal (kPa) | 4.788026 X E -2 |
| pound-force/inch ² (psi) | kilo pascal (kPa) | 6.894757 |
| pound-mass | kilogram (kg) | 4.535924 X E -1 |
| pound-mass-foot ² (moment of inertia) | kilogram-meter ² (kg•m ²) | 4.214011 X E -2 |
| pound-mass/foot ³ | kilogram/meter ³ (kg/m ³) | 1.601846 X E +1 |
| slug | kilogram (kg) | 1.459390 X E +1 |

TABLE OF CONTENTS

| | | |
|------|---|----|
| I. | BACKGROUND ----- | 7 |
| | 1. GENERAL ----- | 7 |
| | 2. MATERIAL BEHAVIOR ----- | 7 |
| | 3. CONFIGURATION CHARACTERISTICS ----- | 9 |
| | 3.1 Side-loaded Tubes ----- | 9 |
| | 3.2 Honeycomb ----- | 10 |
| | 3.3 Axially Loaded Crushed Tubes ----- | 11 |
| | 3.4 Frangible Tubes ----- | 12 |
| | 3.5 Inverting Tubes ----- | 13 |
| | 3.6 Energy Absorbed by Cutting Metal ----- | 13 |
| | 3.7 Beams ----- | 13 |
| | 3.8 Summary, Configurations ----- | 15 |
| II. | THEORETICAL APPROACH ----- | 17 |
| | 4. MACHINE-FOUNDATION-SNUBBER ARRANGEMENT ----- | 17 |
| | 5. VISCOPLASTIC BEAM RESPONSE ----- | 17 |
| III. | EXPERIMENTAL PROCEDURE AND APPARATUS ----- | 18 |
| IV. | RESULTS ----- | 20 |
| | 6. SIDE-LOADED TUBES ----- | 20 |
| | 6.1 Test Results ----- | 20 |
| | 6.2 Theoretical Results ----- | 21 |
| | 7. AXIALLY LOADED CRUSHED TUBES ----- | 22 |
| | 8. HONEYCOMB ----- | 22 |
| | 9. BEAMS ----- | 23 |
| | 9.1 Test Results ----- | 23 |
| | 9.2 Theoretical Results ----- | 24 |
| V. | SUMMARY AND CONCLUSIONS ----- | 27 |
| | REFERENCES ----- | 67 |

LIST OF ILLUSTRATIONS

| Figure | | Page |
|--------|--|------|
| 1 | Various significant stress-strain curves ----- | 29 |
| 2(a) | One-degree-of-freedom representation of a machine and foundation ----- | 30 |
| 2(b) | Bilinear load-displacement relationship for nonlinear snubber spring ----- | 30 |
| 3 | Clamped-clamped beam and support arrangement ----- | 31 |
| 4 | Sketch of IMPAC drop-table shock machine ----- | 32 |
| 5 | Simulated machine-snubber configuration using steel plates and side-loaded rings ----- | 33 |
| 6 | Photographs of deformed specimens----- | 34 |
| | (a) Side-loaded as-received tube | |
| | (b) Side-loaded annealed tube | |
| | (c) Axially loaded crushed tube | |
| | (d) Axially loaded honeycomb | |
| 7 | Stress-strain curves for tensile specimens from as-received and annealed tubing ----- | 35 |
| 8 | Load vs. deformation for a 2" long, side-loaded tube, using Tinius-Olsen machine. (Tube edges cut by tube cutter.) ----- | 36 |
| 9 | Load vs. deformation for four 1/2" long, annealed, side-loaded tubes using Tinius-Olsen machine ----- | 37 |
| 10 | Load vs. deformation for annealed, side-loaded tubes using Tinius-Olsen and shock machines ----- | 38 |
| 11 | Load vs. deformation for annealed, side-loaded tubes for two successive 15" drops ----- | 39 |
| 12 | Load vs. deformation for successive drops 1, 2, 3, 4, & 9 compared with quasistatic curve for side-loaded tubes ----- | 40 |
| 13 | Load vs. deformation for successive drops 1, 2, 3, 4 for side-loaded tubes | 41 |
| 14 | Input acceleration \ddot{y}_0 and transmitted acceleration \ddot{y}_1 versus time for drops 1, 2, 3, & 4 using side-loaded tubes ----- | 42 |
| 15 | Acceleration vs. time, \ddot{y}_0 and \ddot{y}_1 , for drop 9 using side-loaded tubes in machine-snubber configuration ----- | 43 |
| 16 | Relative velocity $(\dot{y}_1 - \dot{y}_0)$ vs. deformation for drops 1, 2, 3, & 4, for side-loaded tubes ----- | 44 |
| 17 | Load rate vs. deformation for 10" drops 1 & 2, for side-loaded tubes ----- | 45 |
| 18 | Theoretical and experimental load-deformation curves for 10" drops 1 & 2, for side-loaded tubes ----- | 46 |
| 19 | Theoretical and experimental acceleration vs. time, \ddot{y}_1 , for 10" drop 1, for side-loaded tubes ----- | 47 |

| | | |
|----|--|----|
| 20 | Theoretical and experimental acceleration vs. time; \ddot{y}_1 , for 10" drop 2, for side-loaded tubes ----- | 48 |
| 21 | Theoretical and experimental load-deformation curves for 15" drop 1, for side-loaded tubes ----- | 49 |
| 22 | Experimental load versus deformation for as-received and annealed tubes loaded axially ----- | 50 |
| 23 | Experimental load versus deformation for aluminum honeycomb ----- | 51 |
| 24 | Experimental load versus deformation for aluminum honeycomb during static loading and unloading ----- | 52 |
| 25 | Experimental load versus deformation for aluminum honeycomb for static pre-crush and then 10" drop 1.----- | 53 |
| 26 | Experimental accelerations, \ddot{y}_0 & \ddot{y}_1 , versus time for aluminum honeycomb for 10" drop 1 after a static pre-crush ----- | 54 |
| 27 | Static stress-strain curves for various steels ----- | 55 |
| 28 | Static load versus central deflection curves for steel beams ----- | 56 |
| 29 | Theoretical dynamic stress-strain curves for WARPLIS ----- | 57 |
| 30 | Load vs. central deflection for WARPLIS beams, dynamic and static loading | 58 |
| 31 | Acceleration-time comparisons for WARPLIS beam, 10 inch drop, 20 msec programmer ----- | 59 |
| 32 | Central deflection vs. time for WARPLIS beam, 14 inch drop, 11 msec programmer ----- | 60 |
| 33 | Strain-time comparisons for WARPLIS beam, 10 inch drop, 20 msec programmer ----- | 61 |
| 34 | Theoretical strain-time for WARPLIS ----- | 62 |
| 35 | Dynamic load-strain comparisons for WARPLIS beam, 14 inch drop, 11 msec programmer ----- | 63 |
| 36 | Theoretical dynamic load vs. moment at support for WARPLIS beam ----- | 64 |
| 37 | Theoretical dynamic stress-strain relations for annealed 1018 steel ----- | 65 |
| 38 | Theoretical dynamic load vs. moment at support for annealed 1018 beam ---- | 66 |

I. BACKGROUND

1. GENERAL

This report summarizes results of the initial phases of an investigation of the application of energy-absorbing foundations for protection of equipment in ships under nuclear weapon attack. The results apply in general to structures submitted to base motion.

There are three parts of the report. First a summary is given of the pertinent publications. Second, an outline is given of analytical procedures used during the first year of the study. Third, experimental and analytical results are given from the first phase of the present study on side-loaded tubing, end-loaded tubing, honeycomb, and beams.

With regard to energy-absorbing foundations, the parameters of particular interest are associated with material behavior and configuration characteristics.

2. MATERIAL BEHAVIOR

The important material properties are elasticity, yield stress, ductility, rate sensitivity, post-yield stiffness, and ultimate strength.

The metals of interest are steel and aluminum. The strain rates are associated with gross structural motions of equipment on their foundations and range up to about 30/sec. The elastic modulus is practically insensitive to such loading rates. A primary effect of rate is the increase in yield strength. Hecker [2] recently summarized experimental studies of yield phenomena in biaxially loaded metals, giving 277 references. Lindholm [3] reviewed methods for conducting tests over the range of strain rates. Steel is typically very strain rate sensitive, while aluminum is much less so. The dependence of the dynamic lower yield stress $\sigma(\dot{\epsilon})$ on the plastic strain rate $\dot{\epsilon}$, for strain rates up to 1000/sec was represented by Cowper and Symonds [4] as the following empirical expression,

$$\frac{\sigma(\dot{\epsilon})}{\sigma_0} = 1 + \left(\frac{\dot{\epsilon}}{D} \right)^{\frac{1}{p}} \quad (1)$$

where σ_0 is the static yield stress, D and p are material constants and p may be taken as an integer. The values $D = 40 \text{ sec}^{-1}$ and $p = 5$ were deduced from data from tension impact tests of steel of Manjoine [5]. For aluminum [6] the values are $D = 6500/\text{sec}$ and $p = 4$. Belsheim [7] discussed dynamic yield stress as related to strain rate and Vigness [8] summarized data relating dynamic yield to "delayed-yield time". The time delay between applied dynamic stress and resulting strain is another important effect which is accounted for to some extent in the constitutive equation proposed by Malvern [9]

$$\dot{\epsilon} = \frac{\dot{\sigma}}{E} + K(\sigma - \sigma_{st})^{\frac{1}{n}} \quad (2)$$

Here ϵ and σ are functions of time, E is Young's modulus, σ_{st} is the static stress for the same strain, and K and n are material parameters. Cristescu [10] suggested a constitutive equation of the type:

$$\dot{\epsilon} = \frac{\dot{\sigma}}{E} + \phi(\sigma, \epsilon) \dot{\sigma} + \Psi(\sigma, \epsilon) \quad (3)$$

where

$$\Psi(\sigma, \epsilon) = \begin{cases} \frac{K(\epsilon)}{E} [\sigma - f(\epsilon)] & \text{if } \sigma > f(\epsilon) \\ 0 & \text{if } \sigma < f(\epsilon) \end{cases} \quad (4)$$

The function ϕ is the measure of the instantaneous plastic response. The $\Psi(\sigma, \epsilon)$ is similar to the second term in equation (1), but it depends on the overstress $[\sigma - f(\epsilon)]$, where $f(\epsilon)$ is the relaxation boundary, below which the response is elastic (see Fig. 1). The relaxation boundary and the static stress-strain curve may not be the same. On the dynamic stress-strain curve in Fig. 1, the maximum stress occurs at B and the maximum strain at C. The time delay between occurrence of maximum stress and maximum strain is the relaxation time.

The type of law in equation (1) applies best to perfectly plastic materials since it relates only to increased yield stress. Perrone [11] suggested a flow law in Equation (5) which accounts for the strain hardening aspects as well as increased yield:

$$\frac{\sigma}{\sigma_0} = \left[1 + \left(\frac{\dot{\epsilon}}{D} \right)^{\frac{1}{n}} \right] [1 + c\epsilon] \quad (5)$$

$$c = f(\dot{\epsilon}) \quad (6)$$

If the strain hardening is a function of strain rate, then equation (6) could be used with (5).

Plass [12] developed a constitutive equation for beam bending by assuming plane sections remain plane after bending and integrating (2) over the beam cross-section, with the result

$$\dot{k} = \frac{\dot{M}}{EI} + R(M - M_{st})^{\frac{1}{n}} \quad (7)$$

Here \dot{k} is curvature rate, M is dynamic moment, EI is bending stiffness, and M_{st} is moment obtained from the static moment-curvature curve.

3. CONFIGURATION CHARACTERISTICS

The important configuration characteristics are energy-absorbing efficiency, elastic stiffness, ultimate deformation, directional properties and transmitted accelerations.

3.1 Side-loaded tubes

The large plastic response of side-loaded tubes under static loading has been studied analytically and experimentally [13, 14]. The deformation δ is related to load P and tube diameter d by

$$P = \frac{P_0}{\sqrt{1 - \left(\frac{\delta}{d}\right)^2}} \quad 0 \leq \delta \leq \frac{d}{\sqrt{2}} \quad (8)$$

The solution ceases to be valid for $\delta > \frac{d}{\sqrt{2}}$. The load P_0 is the load at which the tube begins to deform as a mechanism after formation of plastic hinges at the quarter-points. The load P_0 is related to the fully plastic moment M_0 , the mean radius r , the tube thickness t , and the tube width W by

$$P_0 = \frac{4M_0}{r} = \frac{\sigma_0 t^2 W}{r} \quad (9)$$

For the dynamic behavior of material under uniaxial, impulsive loading Perrone [15] suggested a simplification in the analysis, namely that the initial strain rate could be assumed to be constant throughout the entire flow process. For a pulse loaded structure, it is necessary to estimate the peak strain rate and assume the associated stress to be constant.

For an application of side-loaded rings to highway impact data, Perrone [16] presented stress versus strain rate data for $10^{-2} < \dot{\epsilon} < 400/\text{sec}$ and static load versus deflection curves for tubes of three different types of steel. These tubes were 18 inches in diameter.

With regard to energy absorption, Perrone assumed that the load-deformation curve rose linearly from P_0 at zero deflection to $2P_0$ at deflection equal to $2r$, so that the energy U absorbed is approximately

$$U = 3P_0 r = 12M_0 = 3\sigma_0 t^2 W \quad (10)$$

The result is surprising, since the energy absorbed does not depend on radius of the tube. Rate of loading effects may be taken into account by increasing the yield stress according to equation (1).

It should be noted that in reference [14] it was assumed that the tube was being crushed between parallel plates so that the contact point would move out as the

characteristic peanut shape develops for the tube. In reference [16], the loading appears to be more centrally applied, which results in a softer load-deformation curve for large deformations.

The maximum load carried should occur at maximum deformation, unless the tube fails before that. Failure could occur at the plastic hinges for brittle metals. The suitability of the material can best be determined by tests of the tubing itself.

3.2 Honeycomb

Honeycomb has received considerable attention as an energy-absorbing, cushioning material for protection during air drops of equipment, moon landing of space craft and for many other applications. An excellent tutorial paper on cushioning for aerial delivery was given by Thompson and Ripperger [17].

The materials which have been tested most are paper and aluminum honeycombs. For air drops, the ideal load-deformation curve is flat. One measure of the efficiency for energy absorption is

$$\text{Efficiency} = \frac{U}{\sigma_m x d} \quad \times 100\% \quad (11)$$

where σ_m = maximum stress and d is maximum deformation. Thus a rectangular stress-deformation curve would represent the ideal efficiency of 100%. Paper honeycomb has a nearly ideal stress-strain curve up to about 70% strain, above which it stiffens as it begins to bottom out.

Aluminum honeycomb stress-strain curves typically show an initial sharp stress peak, called the compressive strength, at which buckling begins. As the strain increases further, the stress drops to a nearly constant level, called the crush strength, which is usually about 65 to 70 per cent of the compressive strength. Data sheets are available which list compressive strength, crush strength, shear strength in two directions, and beam shear modulus. A typical aluminum honeycomb may be specified as 3.7 - 3/8 - .0025 which means successively: density in pounds/ft³, cell size in inches, and metal gage in inches.

With regard to analysis, McFarland [18] discussed two possible modes of failure for honeycomb, a crushing mode and a gross shear failure mode. For the crushing mode the energy U_c and force F_c are

$$U_c = \frac{D\sigma_o t^2}{4} \left(2.057 + 12.396 \frac{P_w}{D} \right) \quad (12)$$

$$F_c = \frac{D\sigma_o t^2}{P_w S^2} \left(4.750 + 28.628 \frac{P_w}{D} \right) \quad (13)$$

where

t = cell wall thickness

S = cell minor diameter

$D = S/3^{1/2}$ = width of cell wall

P_w = width of basic panel element [$D/4 \leq P_w \leq D/2$]

The deformation occurs in an accordion-like pattern, with P_w the length of one pleat, measured along the slope, from peak to valley. For shear deformation, using q_0 as yield stress for shear,

$$U_s = 0.433 q_0 t D P_w \quad (14)$$

$$F_s = \frac{1.155 q_0 t}{S} \quad (15)$$

The total energy U and total force F are

$$U = U_c + U_s \quad (16)$$

$$F = F_c + F_s \quad (17)$$

In addition it is noted in [18] that if the ratio $t/S > 0.004$, the gross shear mode failure will occur, rather than the crushing mode. This is undesirable since the energy absorption in the shear mode is less than in the crushing mode for the same t/S ratio.

For aluminum honeycomb, the initial sharp peak in the stress-strain curve is undesirable and may be eliminated [19] by a slight precrushing or pre-dimpling of the surfaces.

3.3 Axially Loaded Crushed Tubes

Axially loaded tubing has been investigated in a crushing mode [20, 21], a "frangible" mode [22], and an inverting mode [23].

The axially loaded tubing in a crushing mode deforms in an accordion-like fashion. The load-deformation curve has a large initial peak and then oscillates about a fairly flat average. The oscillations are due to the successive formation and bottoming out of new pleats.

Shaw [24] studied this type of deformation and attempted to predict the length h of tube involved in one pleat. An Euler instability is assumed to be involved. The buckling load for a slender column of height h with hinged ends constrained to remain vertically aligned is

$$P = \frac{\pi^2 EI}{h^2} \quad (17)$$

If, further, the instability occurs when the tube just becomes plastic, then

$$P = \pi dt \sigma_o \quad (18)$$

Then, using $I = \frac{1}{12} \pi dt^3$, eliminating P gives

$$\frac{h}{t} = \sqrt{\frac{\pi^2 E}{12 \sigma_o}} \quad (19)$$

Shaw said this agreed well with the observed pattern with a mandrel in place, which aided in stabilizing the formation of the pleats. The load was related to deformation x by

$$P = \pi dt \sigma_o \left[\frac{\pi t}{2h} + \frac{h}{2d} \sqrt{\frac{2h}{x} - 1} \right] \quad (20)$$

The minimum value of x for which this equation holds is x_o , the displacement at which the plastic hinge first develops. The value of x_o is

$$\frac{x_o}{h} = \frac{2}{1 + 4 \left(\frac{d}{h}\right)^2 \left(1 - \frac{\pi t}{2h}\right)^2} \quad (21)$$

The approximate outside diameter of the flange formed in one pleat is

$$D = d + h - t \quad (22)$$

The predicted value from these equations agreed well with static test results, but not with dynamic.

3.4 Frangible Tubes

The frangible tube as an energy-absorbing device was studied by McGehee [25,26]. In the fragmenting-tube process, an axial load is applied to one end of the tube while the other end is pressed over a die. The die is shaped so that the portion of the tube in contact with the die is split into segments and the segments are broken into small fragments. A fluctuating force is developed, but the average force is approximately constant.

An empirical equation for the fragmenting stress in ksi for 2024-T3 aluminum-

alloy tubing is given [26] as

$$\sigma_f = \frac{1.90 \sqrt[3]{D_i/r}}{0.7 - t/r} \quad (23)$$

where

σ_f = axial force/area
t = tube thickness
 D_i = inner tube diameter
r = forming radius of die

The range of t/r studied was from 0.333 to 0.644. For t/r less than 0.25 the tube segments split and roll, but do not fragment. It was found for tubing of uniform thickness that the initial force was higher than that required after fragmenting began. To reduce this peak, a 14° taper was used on the tubing thickness at the die end of the tubing.

On page , the energy-absorbing capability of four metals studied as fragmenting tubes in reference [26] is compared with that of aluminum honeycomb [27] and cellular aluminum [28], both in a crushing mode.

3.5 Inverting Tubes

The axially loaded tubing which is inverted is first flared on one end. Then the flared end is rigidly clamped and the tube is turned inside-out by pushing the tube through the flared end. Kroell [23] gave many experimental results for 3003 aluminum, either annealed or half-hard, and a few for mild steel. The load-deflection curves are flat. The specific energy for 3003-H14 aluminum varies from 2000 to 7000 ft-lb/lb for tubing with thickness ranging from .013 to .060 inches and mean diameter varying from 0.8 to 3.0 inches.

3.6 Energy Absorbed by Cutting Metal

In order to increase the axial force, Kroell [23] added "drag" elements around the outside of the tube which scratched the tubing. The total energy lost was up to 2.37 times that lost due to inverting only.

Shaw [24] discussed an energy-absorbing device in which a circular machine tool is designed to simultaneously skin and draw a round bar. For mild steel about 300,000 in. lb. of energy is required to produce one cubic inch of chips; for aluminum about 150,000 in. lb. is required. To save weight, the tube was made thinner and then the crushing mode occurred before the skinning could develop properly. Thus, the weight of the tubing used for skinning, for the same application to automobile bumpers, was greater than that used in an alternate design in which the tube was crushed axially, so it appears that the tube crushed under axially loading absorbs more energy per pound of material.

3.7 Beams

Beams are used to support equipment on ships, but they are usually designed to behave elastically; therefore, their energy-absorbing capacity is not used. Further, the

need to design elastically often leads to the choice of higher yield steels, which tend to be more brittle. Elastic design must be used where final position and alignment must be maintained, but there are situations where permanent deformations would not interfere with the mission of the structure. Therefore, the ability to perform inelastic analysis for ship shock needs to be further developed.

Much has been published on the dynamic plastic behavior of structures. Baker [29] summarized approximate techniques. Jones [30] presented a literature review of the general topic and referred to the following literature surveys: Goldsmith [31] on beams, Rawlings [32] on beams and frames, Symonds [33] on beams, Johnson [34] on beams, frames and plates, Jones et al, [35] on plates and shells, and Lee [36] on beams, plates and shells. Krajcinovic [37] published a survey of exact solutions for the dynamic rigid-plastic behavior of various perfectly plastic structures and also discussed some of the bounding methods.

While many papers have been published, their application is limited because of various assumptions, such as: the material is rigid-perfectly plastic, the load increases monotonically, the load is impulsive, the deflection curve assumes a certain shape, shear effects on yielding and/or on deformation may be ignored, plastic hinges remain a constant length, etc. A more general approach may be achieved through application of numerical methods and finite element techniques, such as that of Witmer, Balmer, Leech, and Pian [38]. They use layers to represent the cross-section of the beam, plate, or shell, lump the mass at discrete points, and do a time-wise integration. This tends to be expensive on the computer, because of the number of nodes and layers required and because the time interval must be small to achieve stability of the numerical solution. Improvements have been discussed by Leech, Witmer, and Pian [39], Morino, Leech, and Witmer [40], and Wu and Witmer [41, 42].

The writer and associates have studied beams bent slightly into the plastic range due to dynamic loading like that occurring in ship shock. Vogel [44] developed a computer approach to analyze beams tested on the Barry shock machine at the Naval Research Laboratory. He accounted for large deflections and used the special form of constitutive equation for beam bending given in Equation (7). Brown [45] suggested values of the parameters in the same equation based on shock machine tests of steel beams having varying amounts of initial cold work. Frick [46] carried out tests on copper-nickel and steel tubing in bending.

Tests of cantilever beams carrying heavy tip masses were made on the Floating Shock Platform using 315.7 beams, with results reported by Butt et.al, [47]. Later, a three-span hollow shaft of 3.125" O. D. was also tested and experimental displacement, velocity, and strain versus time curves were presented [48]. Displacement versus time was predicted using a finite-difference method and an elastic-perfectly plastic moment-

curvature relationship. Bounds of peak displacement were estimated in one case using an energy technique and an input initial velocity distribution.

3.8 Summary, Configurations

While there has been an effort to develop analysis procedures for elastic-plastic beams under ship shock loading, there has been little experience with design of beams deformed into the plastic range on ships. Other configurations have received little attention as energy absorbing foundations or snubbers on ships. Many configurations have been discussed in the guide for selection of elastic shock mounts prepared by Burns [48]. Typical non-linear, elastic, load-deflection curves are given for helical springs, pneumatic cylinders, hydraulic cylinders, air bags and rubber springs. Some shapes are presented which might be used as elastic-plastic springs, including cantilever beams, hinged-hinged beams, side-loaded tubes, and U-shaped mounts. For these four shapes equations are presented for each of the three principal axes for the following: elastic spring constant, elastic deflection, maximum moment and point of maximum stress, load at which yield stress is reached at the most highly stressed point, and load at which most highly stressed section becomes fully plastic. Thus the guide is useful for designing elastic-plastic shock mounts deformed slightly into the plastic range.

The use of energy-absorbing configurations for collision protection of ships was surveyed by Jones [49]. He compared the energy-absorbing capability of foam-filled honeycomb with that of deck plating. A nest of tubes which would be crushed axially was also suggested and some approximate formulas were given for energy-absorbing capabilities of the configurations. While the problem is different from that of the present study, some of the information on configurations is applicable.

When considering configurations for protection of internal ship or submarine equipment against shock, the fact that the shock may occur in any direction must be considered. Axially loaded tubes as shock snubbers oriented in three principal directions may be satisfactory, provided the tubes are guided on mandrels to assure that the tubes deform axially, but developing such a system may be difficult. Side-loaded tubes and honeycomb have an advantage because of their directional properties, so these configurations have been considered first in the present study.

Energy-absorbing capability of various configurations were compared by Perrone [50]. His summary, along with data from reference [26] is given in Table 2.

Table 2. Energy Absorbing Systems

| System | Specific Energy | |
|---|---|--|
| | $\frac{\text{ft. lb.}}{\text{lb.}} \times 10^3$ | Comments |
| Inverting tubes [50] | 2 to 4 | Aluminum, 3" O. D., .035" wall thickness |
| Cellular aluminum [50] | 1 to 7 | |
| Aluminum honeycomb [50] | 1 to 8 | Strain dependent, ranges up to 70 percent strain |
| Foam-filled honeycomb [50] | 3 to 8 | |
| Side-loaded tube [50] | 0.5 to 1.5 | $\frac{r}{t} > 5$ |
| Side-loaded tube (Sandwich) [50] | 1.5 to 5 | |
| Frame assembly [50] | 0.3 to 0.5 | |
| Frangible tube [26] | | |
| AZ 31 B Magnesium alloy | 14 | |
| 2024-Ts Aluminum alloy | 30 | |
| 7075-T6 Aluminum alloy | 33.5 | |
| AISI 4130 Steel tubing | 38.5 | Cold water quenched |
| Axially loaded crushed tube [Present Study] | | |
| Annealed 1018 steel | 10 | 2" O. D., .0625" wall thickness |

II. THEORETICAL APPROACH

4. MACHINE-FOUNDATION-SNUBBER ARRANGEMENT

The goal of the analysis is to be able to predict the response of a machine-foundation-spring-dashpot combination to a base motion input. If the base motion is translational, the system may be represented by the one-degree-of-freedom system shown in Figure 2(a). During normal operation the machine may be supported on a linear spring and dashpot to attenuate steady vibration. Then, during a severe shock applied as base motion at the support, the shock snubber comes into contact with the mass. A representation of the load-deflection behavior of the snubber is shown in Figure 2(b). The idealized curve used in the first phase of the analysis is assumed to have an elastic portion of stiffness k_e . After a yield load is reached, the slope of the curve changes to k_p . When unloading begins, it is assumed to occur elastically, so the stiffness is again k_e . The differential equations of motion are

$$m\ddot{y}_1 + k(y_1 - y_0) + c(\dot{y}_1 - \dot{y}_0) = -L(t) - mg \quad (y_1 - y_0) \geq a \quad (24)$$

$$k(y_0 - y_1) + c(\dot{y}_0 - \dot{y}_1) = L(t) + R(t) \quad (y_1 - y_0) \geq a \quad (25)$$

For $(y_1 - y_0) < a$, there is no contact with the snubber and $L(t) = 0$.

Equation (25) was used to predict the response of a mass supported on a set of side-loaded tubes. The clearance, a , was taken as zero. The yield load and the stiffnesses k_e and k_p were obtained from experimental data. The solution was developed using a finite difference approach with central differences.

5. VISCOPLASTIC BEAM RESPONSE.

The beam analyzed was rigidly clamped at each end such that the supports could neither rotate nor move axially (Figure 3). The support was submitted to a vertical base motion in a shock machine. The beam carried a heavy central mass. The maximum deflections were about five times the beams thickness. Both bending and axial deformation were taken into account. The procedure used was that developed by Witmer et al., in reference [38]. The beam thickness is represented by layers, with each layer having the constitutive relationship of equation (2) with $n = 1$, or

$$\dot{\epsilon} = \frac{\dot{\sigma}}{E} + K(\sigma - \sigma_{st}) \quad (26)$$

The procedure is outlined in a doctoral thesis by S. J. Yim [51], so the details are not repeated here. Some significant results of the study are presented in the Section IV.

III. EXPERIMENTAL PROCEDURE AND APPARATUS

The purpose of the experiments was two-fold. First, load-deformation curves were found at various loading rates. Second, the attenuation produced by using energy-absorbing snubbers was demonstrated.

The procedure was to determine the material and configuration behavior at low and moderate loading rates in a conventional Tinius-Olsen testing machine. An apparatus was then designed so that the configuration could be tested in a simulated machine-snubber arrangement at a high rate in a drop-table shock machine.

The instrumentation used to obtain load-deformation records with the Tinius-Olsen test machine was that incorporated in the machine. The maximum deformation rate obtainable is 20 inches/minute.

A sketch of the IMPAC shock machine is shown in Figure 4. The machine consists of a heavy, 220 pound table on which the specimens are mounted. The table is raised to a specified height, from which it is dropped. The impact is controlled by a spring-like "programmer" on the bottom of the table. After the programmer contacts the rigid base, the table undergoes a severe negative acceleration. The acceleration-time curve is approximately a half-sine wave with durations of 5 to 25 milliseconds obtainable and maximum accelerations of 100g. After rebound, the table moves freely upward, guided by the side rails. At the top of the rebound, air brakes are automatically activated which press against the rails and stop the table, preventing a second impact.

A simulated machine-snubber configuration on the shock machine table is shown in Figure 5. The machine is simulated by two steel plates, each 8" x 1/2" x 8-3/4". The plates were bolted together to form a single mass, and the total weight was 20 pounds. The snubbers shown are four side-loaded rings in a symmetrical arrangement. The plate and rings were kept in place by tape which held the configuration in position during the free fall, but slackened and allowed the plate to separate from the rings upon rebound.

Three accelerometers were attached to the top of the plate, at locations A, B and C in Figure 5. By this arrangement the vertical acceleration of the mass was measured, as well as rotational acceleration about two perpendicular principal axes through the center of the top surface of the mass. A fourth accelerometer was glued to the top of the shock machine table, to measure input acceleration \ddot{y}_0 . Two accelerometers were Kistler 808A with Kistler 545A charge amplifiers. The other two accelerometers were Endevco 2222B with Endevco 2730 charge amplifiers.

For the beam tests, the two Kistler accelerometers were used to measure vertical acceleration, one on the central mass and one on the shock machine table. The unsupported length of the beam was 8" (Figure 3). Strain gauges were located on top and bottom of the beam at distances of 1/2", 1", 2", and 3" from the support. The beam arrangement was also

tested statically in the Tinius-Olsen test machine. The strain gauges were Micromasurement EP-08-125BB-120.

IV. RESULTS

Tests results were obtained for side-loaded tubes, end-loaded tubes, honeycomb, and beams. Analysis was carried out for side-loaded tubes and beams.

6. SIDE-LOADED TUBES

6.1 Test Results

The tubes tested were all obtained from one piece of round seamless mechanical tubing of cold drawn carbon steel, with 0.10 - 0.25% carbon. The wall thickness was 16 gauge or 0.065 inches, and the outside diameter was 2 inches. Some of the tubing was annealed, after it was found that the as-received tended to crack at the plastic hinges at large deformations (see Figure 6(a)).

Small tensile specimens were cut from the tubing with the axis of the specimens in the direction of the axis of the tubing. The specimens had a slight curvature and the ends were flattened in the grips, but this was thought to have little effect on the tensile properties. The results are shown in Figure 7. The annealed material had a definite yield at 44,000 psi.

Specimens 2" long were cut from the as-received tubing in a non-ideal, but practical, way by using a plumber's tube-cutter. This produced a v-shaped groove. The tubing was tested in the Tinius-Olsen machine at varying rates. Plastic hinges tend to develop, first on the top and bottom and then on the sides of the tubing, so finally there are four hinges located at 90° intervals around the tube circumference (see Figure 6(b)). All the as-received tubes developed cracks at about one inch deformation. On Figure 8, a load-deformation curve is shown at a loading rate of 20"/min. A sudden, temporary, loss of stiffness occurred when the cracks developed. This tubing was judged to be unacceptable in the as-received state and all subsequent tests were done on annealed tubing. Test results for annealed tubing at two rates are shown in Figure 8. The varying slopes of the initial elastic portion of the curves were due in part to the raised edges produced by the tube-cutter. Specimens for later tests were cut and had edges machined on a lathe.

In the shock machine, four 1/2" long tubes were used, rather than one 2" long tube. Test results for four side-loaded annealed tubes are shown in Figure 9, for two different sets of tubes, to check repeatability, at a loading rate of 0.05"/min. The load-deformation curve for four 1/2" long tubes was practically identical to that of one 2" long tube, at the same loading rate.

In Figure 10 the load versus deformation curves of four 1/2" tubes are shown as obtained from the Tinius-Olsen machine at 0.05"/min. and 0.3"/min. Also shown are the load-deformation curves obtained on the shock machine due to two successive 15" drops. As expected, because of rate effects, there is an increase in yield load as loading rate increases.

The deformations from shock machine data were obtained by double integration of $(\ddot{y}_1 - \ddot{y}_0)$. The dynamic loads are $(m\ddot{y}_1 - mg)$. For the data plotted, the angular acceleration of the mass was small enough to be neglected. In Figure 11, the load-deformation curves for the successive drops are plotted with the curve for the second drop shifted to the origin. Note that the load-deformations curve is nearly flat for the first drop, but the configuration is stiffer during the second drop.

In another set of shock machine tests, a set of four 1/2" long annealed tubes was submitted to eight successive 10" drops and then a 15" drop. Resulting load-deformation curves for Drops 1 through 4 and Drop 9 are shown in Figure 12 and compared with a curve at 0.05"/min. deformation rate on the Tinius-Olsen.

The shifted curves for Drops 1 through 4 are shown in Figure 13. Less energy is absorbed on each successive drop.

Transmitted acceleration is compared with base acceleration in Figure 14 for the first four 10" drops. For the first drop the maximum transmitted acceleration, \ddot{y}_1 , is about 26 g compared to a peak base acceleration, \ddot{y}_0 , of 45 g. However, by the fourth drop, the tubes furnished no attenuation.

In Figure 15, the transmitted acceleration is compared with input acceleration for the 9th drop. Here the peak input acceleration is 58 g and the maximum transmitted is 67 g.

The relative velocity versus deformation for the four successive 10" drops is shown in Figure 16. These appear to be almost semi-circular during the compressive phase for the rings. The calculated rebound (positive) velocity is shown and seems to vary only slightly on successive drops.

Load rate versus deformation for the first two successive 10" drops are shown in Figure 17. The load rate is practically zero except at the beginning and the end of the deformation stroke. This may have some significance in developing an approximate analysis procedure.

6.2 Theoretical Results

In Figure 18, predicted load-deformation curves are compared with those from measurements. To predict the results, an equation based on (24) was used, with $y_r = y_1 - y_0$

$$m\ddot{y}_1 + L(t) = -mg \quad (27)$$

$$\text{or } m\ddot{y}_r + L(t) = -mg - m\ddot{y}_0$$

The $L(t)$ curve was a bi-linear curve, as in Figure 2(b), which was estimated from test data from the Tinius-Olsen machine, but with the yield increased to account for

rate effects. The input was the measured \ddot{y}_0 . Agreement is good except for the unloading curve and the residual deformation for Drop 2.

Predicted acceleration versus time is given in Figure 19 for 10" Drop 1 and in Figure 20 for 10" Drop 2. In Figure 20, the effect is studied of doubling the theoretical elastic stiffness k_e of the tubing. The $k_e = 8300$ lb./in. produces the better fit.

A comparison of theoretical and experimental load-deformation curves for the first of two successive 15" drops is shown in Figure 21. The simple representation is again fairly adequate except during unloading, where the predicted residual deformation is in error by about 8%.

In general, predictions are good for side-loaded tubing, but could be improved by incorporating a constitutive equation of the form of equation (26).

7. AXIALLY LOADED CRUSHED TUBES

Several tests were run at moderate loading rates in the Tinius-Olsen machine of the 2" diameter steel tubing under axial loading. A typical load-deformation curve for an as-received, 2" long tube is shown in Figure 22, in comparison with that for an annealed tube of the same size. The ends of the as-received tube were cut with a tube-cutter, while those of the annealed tube were machined square. The end conditions affect the initial shape of the curve, until the end starts to curl in and the first pleat begins to form. The deformed, annealed tube is shown in Figure 6(c), showing two well-formed pleats. The pleats develop successively and the rise and fall of the load-deformation curve is associated with the formation of successive peaks.

8. HONEYCOMB

Experiments were performed on aluminum, 5052 alloy honeycomb donated by American Cyanamid Corporation. The honeycomb was military grade, density 3.7 lb./ft³, 3/8" core, 0.0025 metal gage, and 5/8" deep. The crush strength is published as 290 psi and compressive strength as 200 psi. A quasi-static load-deformation curve from the Tinius-Olsen machine of a 2" x 2" specimen is shown in Figure 23. There were thirty complete cells. A photograph of a typical deformed specimen is shown in Figure 6(d). The inner cells deformed by the formation of successive pleats, much as the axially crushed tube shown in Figure 6(c). Three pleats can be seen in Figure 6(d). The outer walls buckle in a mode involving the total depth of the specimen. The initial peak or crush strength is higher than 4 in² x 290 psi expected from the advertised value but the advertised compressive strength of 4 in² x 200 psi is close to the average after the first peak.

The initial high peak in the load-deformation curve is undesirable in a shock snubber, since it leads to a high transmitted acceleration. To avoid this peak in the shock machine tests, it was decided to pre-crush the honeycomb in the Tinius-Olsen machine. In Figure 24, a load-deformation curve is shown during a quasi-static pre-crush of a

2" x 1-3/4" honeycomb specimen with twenty-five complete cells. Here the pre-crush was terminated prematurely after about 0.015" deformation, and an undesirable peak of 1200 lb. occurred on re-loading. The best procedure is to continue the pre-crush until the load drops to the average level at about 650 psi. The subsequent oscillation in the load-deformation curve is assumed to be due to the successive formation of pleats. That they formed successively and not simultaneously could not be observed on the present tests, because the pleats formed only on interior cells.

After the pre-crushing procedure was established a 2" x 2" specimen with thirty complete cells was pre-crushed and then used as the snubber in the machine-snubber configuration in the shock machine. The machine was simulated by the same plates, weighing 20 lb., shown in Figure 5. The honeycomb was substituted for the side-loaded rings, but the single specimen of honeycomb was positioned under the center of the plates. In Figure 25, the load-deformation curve is shown for the static pre-crush and the subsequent 10" drop on the shock machine. The measured acceleration-time curves for the 10" drop are shown in Figure 26. The base acceleration \ddot{y}_0 of the shock machine table is compared with the acceleration \ddot{y}_1 transmitted to the plates. Some protection is furnished by the honeycomb, but more could have been achieved by using a honeycomb specimen with a smaller area.

9. BEAMS

This section is a brief summary of some of the results presented in the doctoral thesis of S. J. Yim [51].

9.1 Test Results for Beams

Steel beams were tested in the arrangement shown in Figure 3. The beams were rectangular bars 1" x 1/8" x 18". At each end the beam was clamped in 3" long clamping blocks. The beam carried a central mass made up of four 3" x 4", 1-7/16" thick steel blocks clamped to the beam midpoint. The total weight of the central mass and six bolts and nuts was 20 lb.

The beam materials were WARPLIS and 1018 steel. The chemical composition of WARPLIS is as follows:

| | | |
|-----------|-----------|---|
| Carbon | 0.85-0.95 | % |
| Manganese | 1.00-1.25 | |
| Silicon | 0.15-0.35 | |
| Chromium | 0.40-0.60 | |
| Tungsten | 0.40-0.60 | |
| Vanadium | 0.15-0.25 | |

Beams of 1018 steel were obtained in three conditions: Cold-rolled, hot-rolled, and annealed at 1200°F for 2 hours and 20 minutes and allowed to cool in the furnace for 17 hours.

Results of simple tension tests of the four beam materials are shown as stress-

strain curves in Figure 27. WARPLIS and the cold-rolled 1018 do not have definite yield points and exhibit strain hardening. The hot-rolled and annealed 1018 have sharp yields and then a flat stress-strain curve.

Beams were first clamped in the rig of Figure 3 and tested in the Tinius-Olsen testing machine to obtain quasi-static load-deflection and load-strain curves. Typical experimental static load versus central deflection curves are shown in Figure 28 for WARPLIS and for annealed and hot-rolled 1018 steels. Then dynamic tests were done with the beams in the test rig on the drop table shock machine. New beams were used in each static and dynamic test so that the material experienced first loading in each test.

The quantities measured in the shock machine tests were: absolute acceleration of the central mass, designated \ddot{y}_1 ; absolute acceleration of the base, \ddot{y}_0 ; and strains at various stations. Dynamic loads on the beam were taken as $(m\ddot{y}_1 + mg)$. The relative velocity $(\dot{y}_1 - \dot{y}_0)$ and the relative displacement $(y_1 - y_0)$ of the beam mass relative to the base were obtained by numerical integration of the relative acceleration $(\ddot{y}_1 - \ddot{y}_0)$.

For WARPLIS, dynamic load versus central deflection is shown in Figure 30. The dynamic curve is higher than the static curve, indicating that the material is sensitive to rate of loading and was stiffer during the dynamic tests.

Experimental values of \ddot{y}_1 and \ddot{y}_0 versus time are shown in Figure 31. The maximum acceleration of the mass is about twice that of the base, showing that the beam does not protect the mass.

Experimental deflection versus time, strain versus time and load versus strain are shown in Figures 32, 33 and 35 respectively. These are compared with theoretical predictions, which are discussed in the next section.

9.2 Theoretical Results for Beams

The theoretical results were obtained using the analytical procedure described briefly in Section II.5 and in detail in Reference [51]. The stress-strain relationship used is that of Equation (26)

$$\dot{\epsilon} = \frac{\dot{\sigma}}{E} + K(\sigma - \sigma_{st}) \quad (26)$$

Here σ_{st} is the static stress existing at a certain strain level. In the analysis σ_{st} vs. ϵ was taken as a bilinear curve. When K is very large and the rate terms are small, σ approaches σ_{st} . This is shown in some typical theoretical dynamic stress-strain curves in Figure 29 for WARPLIS. When $K = 5 \times 10^{-3} \frac{\text{in}^2}{\text{lb}\cdot\text{sec}^2}$, a large value, the dynamic curve follows the bilinear static curve. When $K = 5 \times 10^{-7} \frac{\text{in}^2}{\text{lb}\cdot\text{sec}^2}$, a small value, the rate terms dominate and the dynamic curve tends to follow the elastic curve, $\sigma = E\epsilon$. The range of K values between these extremes produces curves such as that of Figure 29 for $K = 5 \times 10^{-5} \frac{\text{in}^2}{\text{lb}\cdot\text{sec}^2}$.

the value which seemed best for WARPLIS. These curves are obtained for a dynamic analysis at a beam location one inch from the clamp and in the top fibers, so the strain rate varied considerably during the loading. The stress-strain curve varies with strain rate, so it will be different at each beam location and each layer on the cross-section.

Theoretical dynamic load versus central deflection is shown for WARPLIS with $K = 5 \times 10^{-5} \frac{\text{in}^2}{\text{lb}\cdot\text{sec}}$ in Figure 30. The agreement with experimental results is very good. The measured base acceleration, \ddot{y}_0 , was used as input for the analysis. Theoretical acceleration-time, central deflection-time and strain-time curves are compared with experimental in Figures 31, 32, and 33 respectively. Agreement for accelerations and deflections is very good, and fairly good for strains. Strains are the most difficult to predict, because they depend on the second derivative of deflection. The location of strain of Figure 33 was top and bottom of the beam, 1" from the support. The beam deflected downward, so the top fiber is in tension and the strain is positive. The lower fibers are first in compression (negative strain). The beam deformation is primarily in bending during the first few milliseconds. However, tension then begins to develop due to the axial restraint of the end clamps. If plane sections remain plane, then the axial or tensile strain at the mid-fiber would be the average of the strains at the top and bottom fibers. It is seen in Figure 33 that the average is zero initially, but that considerable axial strain then develops. The axial strain is associated with string-like behavior of the beam.

In Figure 34, theoretical strain-time curves are shown for the top layer and 1" from the beam clamp for different values of K . At this station, the strain is relatively insensitive to K .

In Figure 35, theoretical and experimental load versus strain curves are compared at the top and bottom fibers 1" from the beam clamp. The average of the two strains at a certain load level would be the axial strain. It is seen that static and dynamic curves are quite close, indicating little rate of loading effect. The theoretical dynamic tensile strain becomes too large, and bending strain prediction is less accurate than axial strain prediction.

In Figure 36, theoretical dynamic load versus moment at the support is shown for WARPLIS beams with different values of K and different values of σ_{dy}/σ_0 which is dynamic yield stress over static yield stress. A plastic hinge develops at the support but, due to strain hardening, the associated bending moment continues to increase until unloading begins to occur.

In Figure 37, theoretical dynamic stress-strain curves are shown for annealed 1018 steel for different values of K . The bilinear static curve was taken as elastic, perfectly plastic. A primary effect of high rate of loading on the annealed steel is to increase the yield stress. If the material then remains perfectly plastic, the most reasonable representation of the shape of the stress strain curve may be obtained by taking

$\sigma_{dy} = 1.5 \sigma_o$ and $K = 5 \times 10^{-1} \frac{\text{in}^2}{\text{lb}\cdot\text{sec}}$, a very large value of K . The difficulty with this representation is that it does not accurately predict the relaxation time, or the time delay between maximum stress and maximum strain.

In Figure 38, the theoretical dynamic moment at the support is shown for annealed 1018 steel for different value of K and σ_{dy}/σ_o . For predicting response of annealed 1018 steel, the best fits occurred for $K = 5 \times 10^{-1} \frac{\text{in}^2}{\text{lb}\cdot\text{sec}}$ with $\sigma_{dy} = 1.5 \sigma_o$. Accuracy of strain predictions for annealed 1018 was poor, due apparently to the unstable nature of the material and the tendency for localized flow to occur. However, accuracy of prediction of accelerations and deflections for all 1018 beams was comparable to that for WARPLIS.

V. SUMMARY AND CONCLUSIONS

The study is concerned with the development of analytical methods for design of energy-absorbing foundations for protection of equipment in ships under nuclear weapon attack. The first part of the study involved looking for suitable configurations and for appropriate representation of material behavior.

There is a great amount of literature dealing with dynamic behavior of materials, but more work needs to be done, especially on unloading and reloading behavior of metals. However, enough is known so that it is possible to estimate the energy absorbed per unit volume of material. To arrive at an approximate bilinear static stress-strain curve, one must know the elastic modulus, the yield stress, and the plastic modulus. To extend to dynamic behavior, the yield stress and plastic modulus must be known as a function of strain rate. The increase in yield stress may be estimated from Equation (1), but it may be necessary to perform several tests at different strain rates to determine the material parameters. For a dynamic stress-strain-time relationships, Equations (2) and (3) may be used, again with the help of tests to determine the parameters for certain materials. Material parameters, test techniques, and related references are discussed in Section I. In addition, the list of Supplemental References gives 362 references related to constitutive equations for dynamic loading and their applications to various structural systems.

With regard to configurations, axially loaded crushed tubes, frangible tubes and inverting tubes are efficient energy absorbers but they must be carefully loaded or guided with a mandrel, so they may be difficult to apply to ship shock where the input may come from any direction.

Side-loaded tubes and honeycomb show promise for use in ship foundations as energy absorbers. In Table 2, page 15, it can be seen that honeycomb is a more efficient energy absorber on a ft.lb./lb. basis. However, honeycomb is more expensive. Further, side-loaded tubes could possibly be straightened in place after an impact, and be re-shocked.

Test results from the present study for side-loaded tubes demonstrate that shock attenuation can be achieved on the shock machine. Further, if desired, the tubes could be designed to absorb energy on two successive shocks. The dynamic load-deflection curve rises to twice the yield load at a deformation of 60% of the tube diameter, as shown in Figure 12, for the annealed tubes. Honeycomb has, on the average, a flatter load-deformation curve after a first, undesirable, sharp peak. This initial peak can be eliminated by pre-crushing or dimpling the honeycomb. A further trait of honeycomb, which may be undesirable, is the slight oscillation of the load-deformation curve about the average line as the successive pleats form.

Beams are used to support equipment on ships. Also, much of the piping on a ship deforms laterally, like a beam. It is important to develop dynamic analysis procedures for beams to account for plastic deformation. Some of the work completed in part

in the present study and in a related thesis [51] shows that a moment-curvature-time relationship of the form of Equation (7) can be used successfully to predict beam response. In addition, values are suggested for R , n , and M_{st} for WARPLIS and for 1018 steel. The 1018 steel was studied in the cold-rolled, hot-rolled, and the annealed conditions. Transmitted timewise accelerations and deflections were accurately predicted for all four steels under shock machine loading. Strain versus time were predicted with good accuracy for WARPLIS and cold-rolled 1018, but with poor accuracy for hot-rolled and annealed 1018.

For shock attenuation, beams are not the best choice, because the load-deflection curve rises rapidly. A good arrangement would be a machine on a bed-plate, protected by energy-absorbing tubes or honeycomb. This system could, in turn, be supported on a foundation which is attached to the hull. It should be noted that the energy-absorbing tubes or honeycomb act as a mechanical fuse and limit the force the machine applies to the foundation, as well as vice-versa. Thus, the use of energy absorbers could result in lighter foundations and equipment or it could lead to in systems which could sustain a more severe attack.

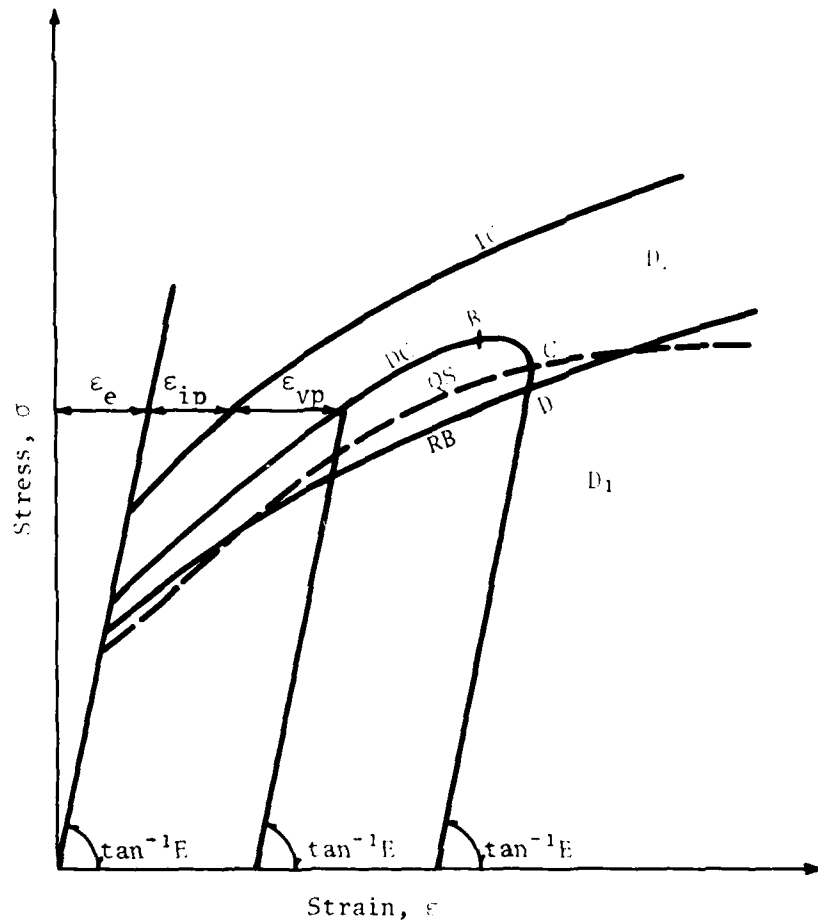


Figure 1. Various significant stress-strain curves: RB, relaxation boundary; QS, quasi-static stress-strain curve; DC, typical dynamic stress-strain curve; IC, instantaneous curve; D_1 , elastic domain; D_2 , domain of possible dynamic stress and strain states. (from Cristescu, ref. [10]).

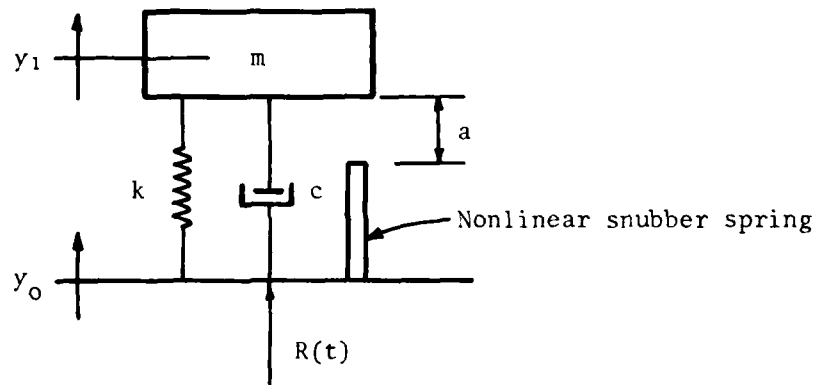


Figure 2 (a). One-degree-of-freedom representation of a machine and foundation.

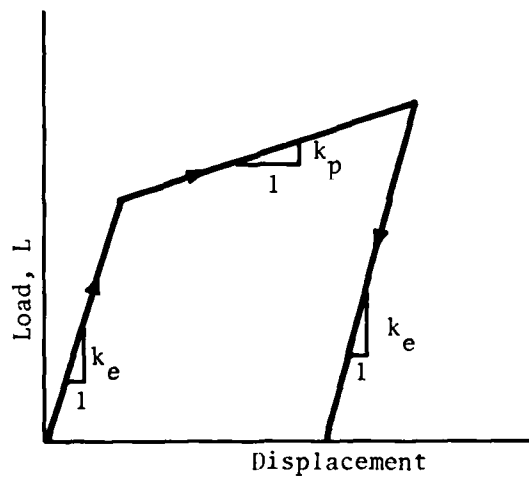


Figure 2(b). Bilinear load-displacement relationship for non-linear snubber spring.

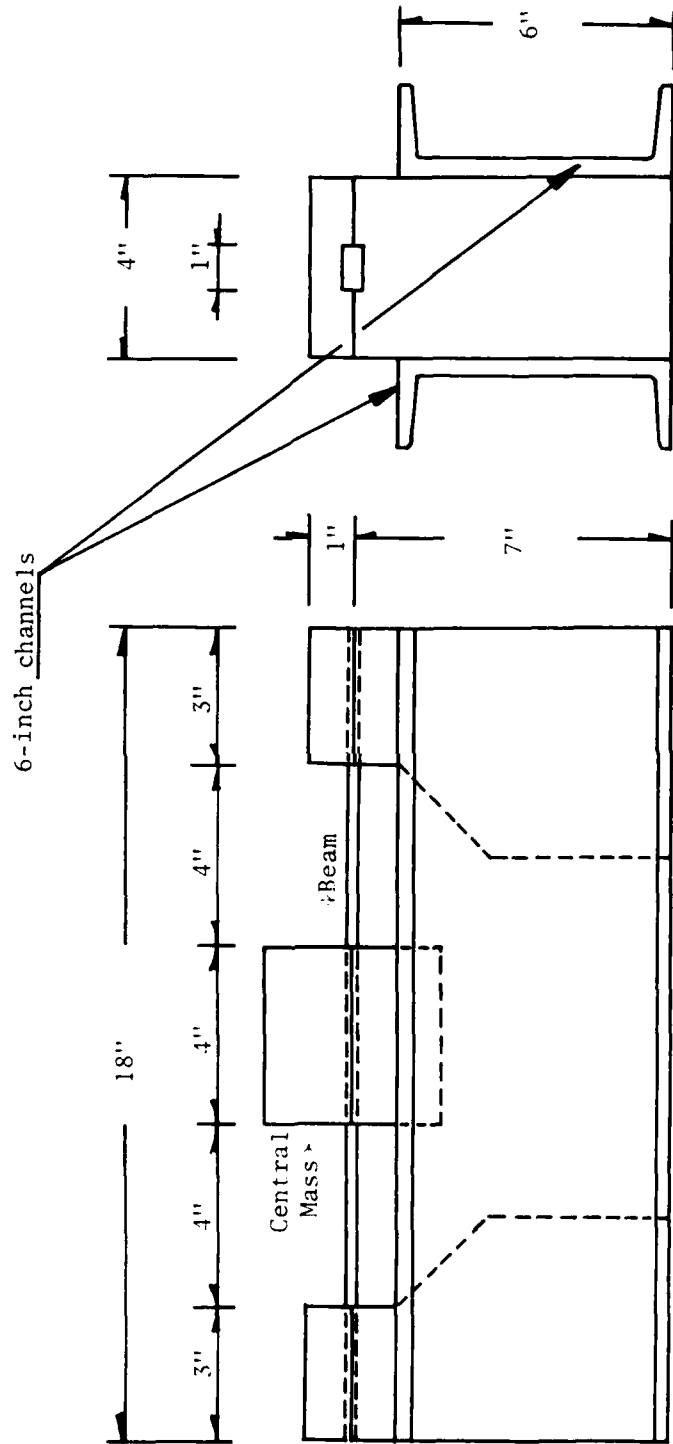


Figure 3. Clamped-clamped beam and support arrangement.

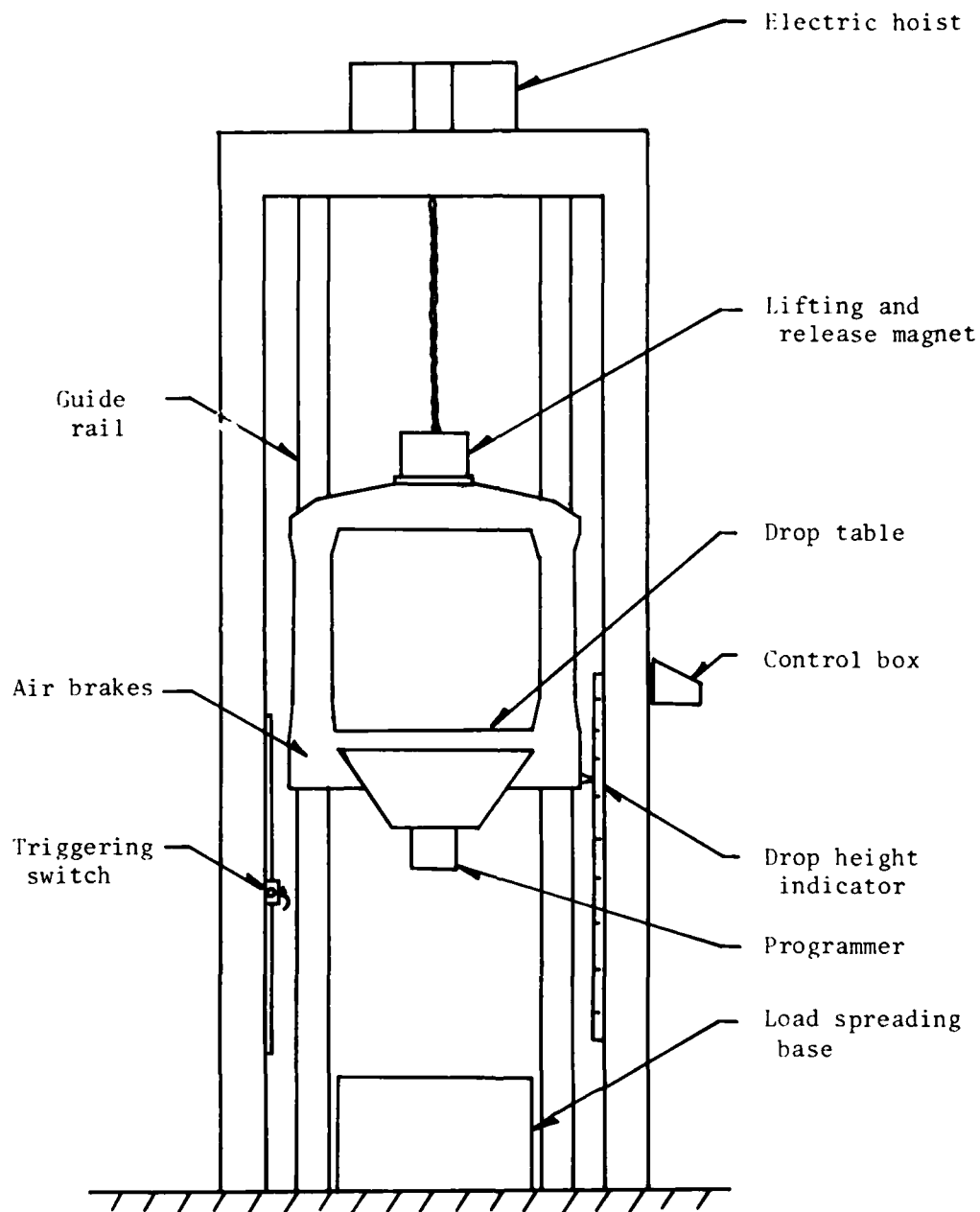


Figure 4. Sketch of IMPAC drop-table shock machine.

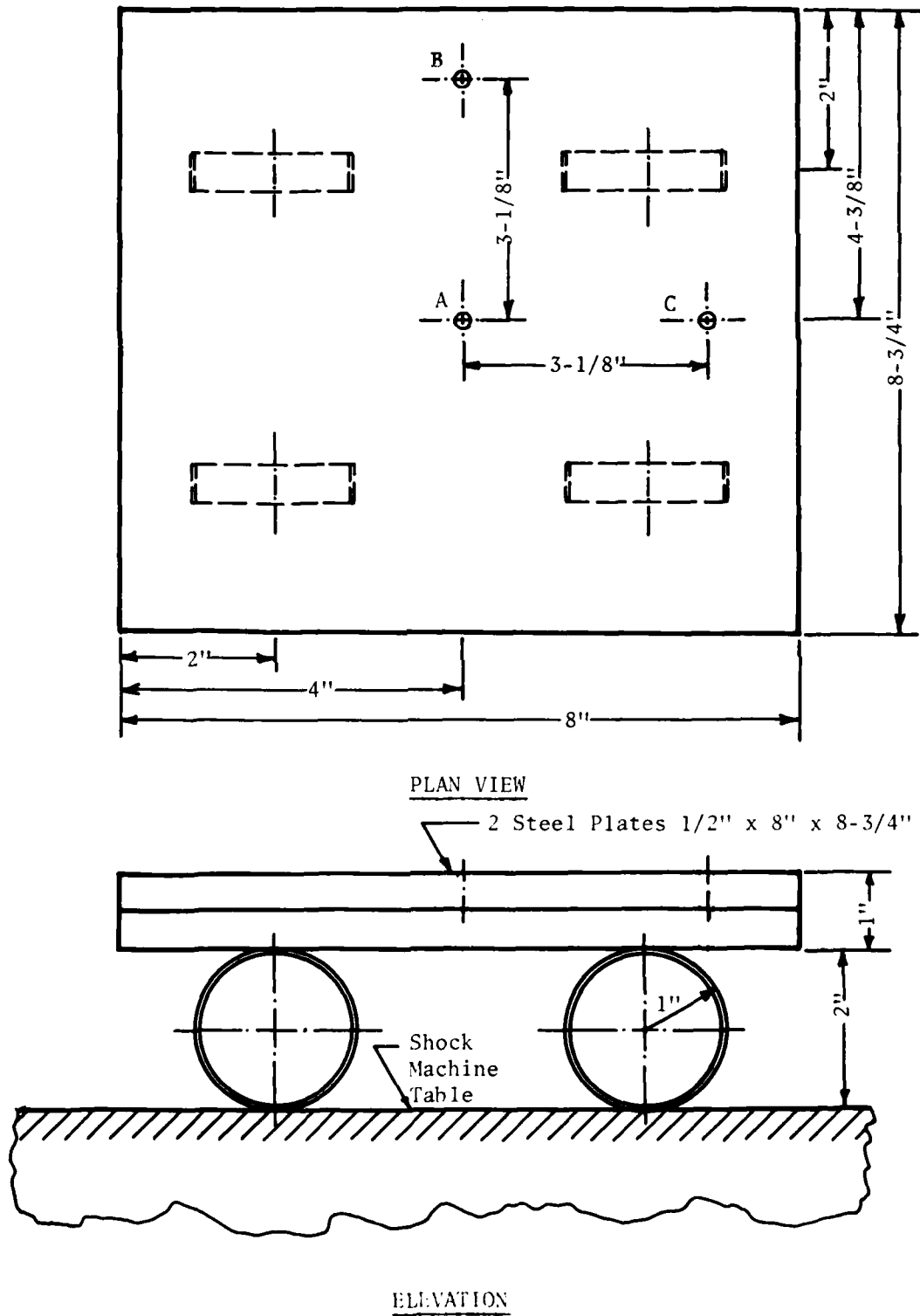


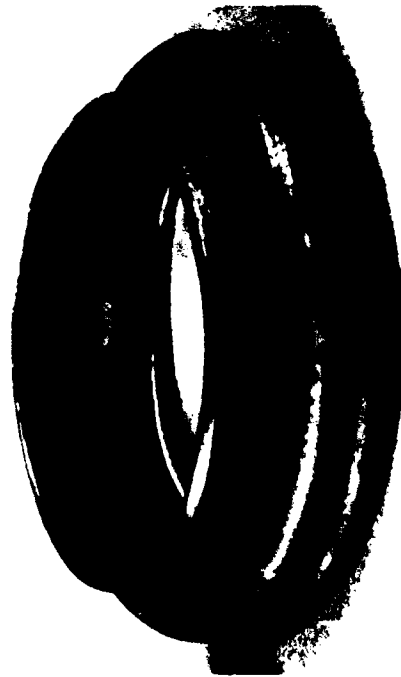
Figure 5. Simulated machine-snubber configuration using steel plates and side-loaded rings.



(a) Side-loaded as-received tube



(b) Side-loaded annealed tube



(c) Axially loaded crushed tube



(d) Axially loaded honeycomb

Figure 6. Photographs of deformed specimens.

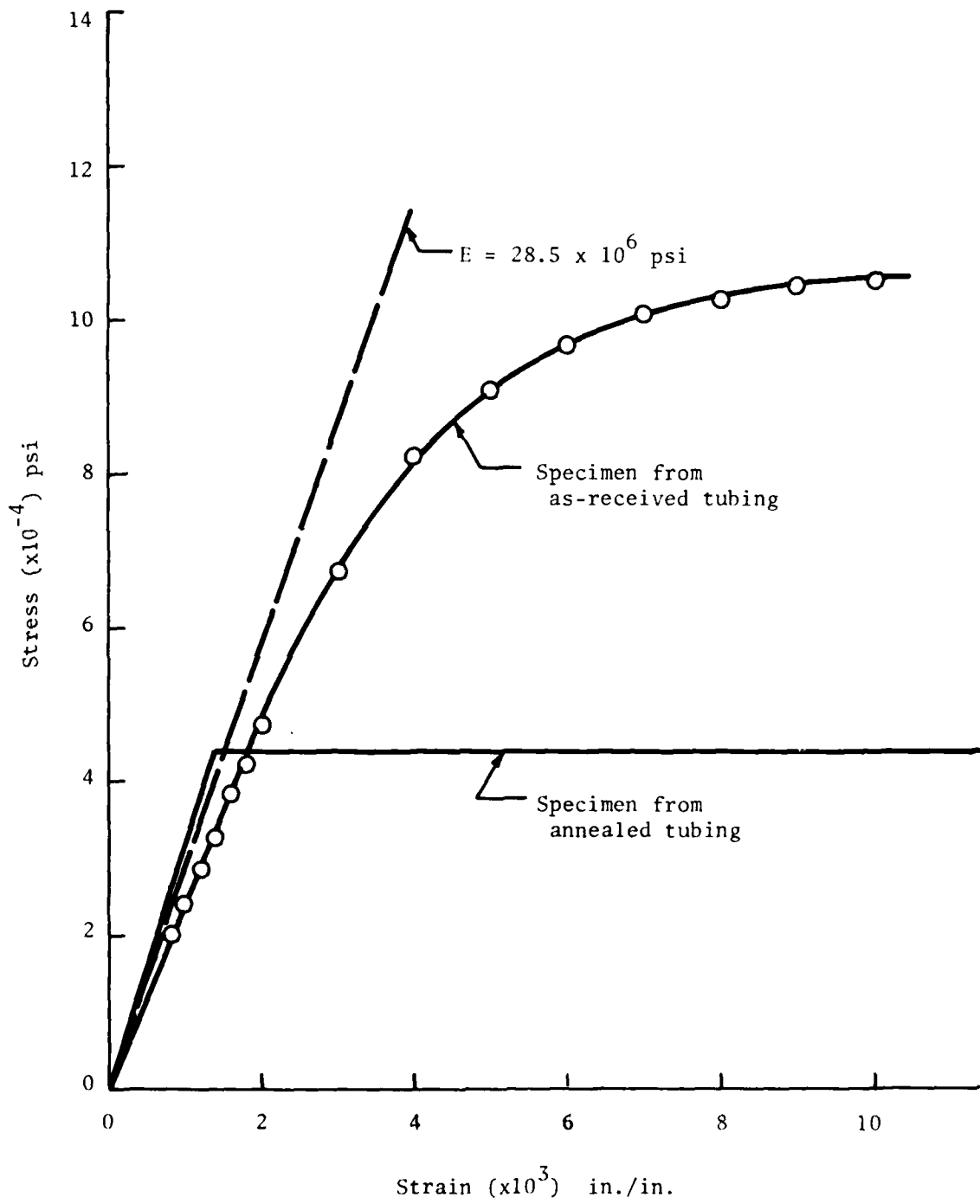


Figure 7. Stress-strain curves for tensile specimens from as-received and annealed tubing.

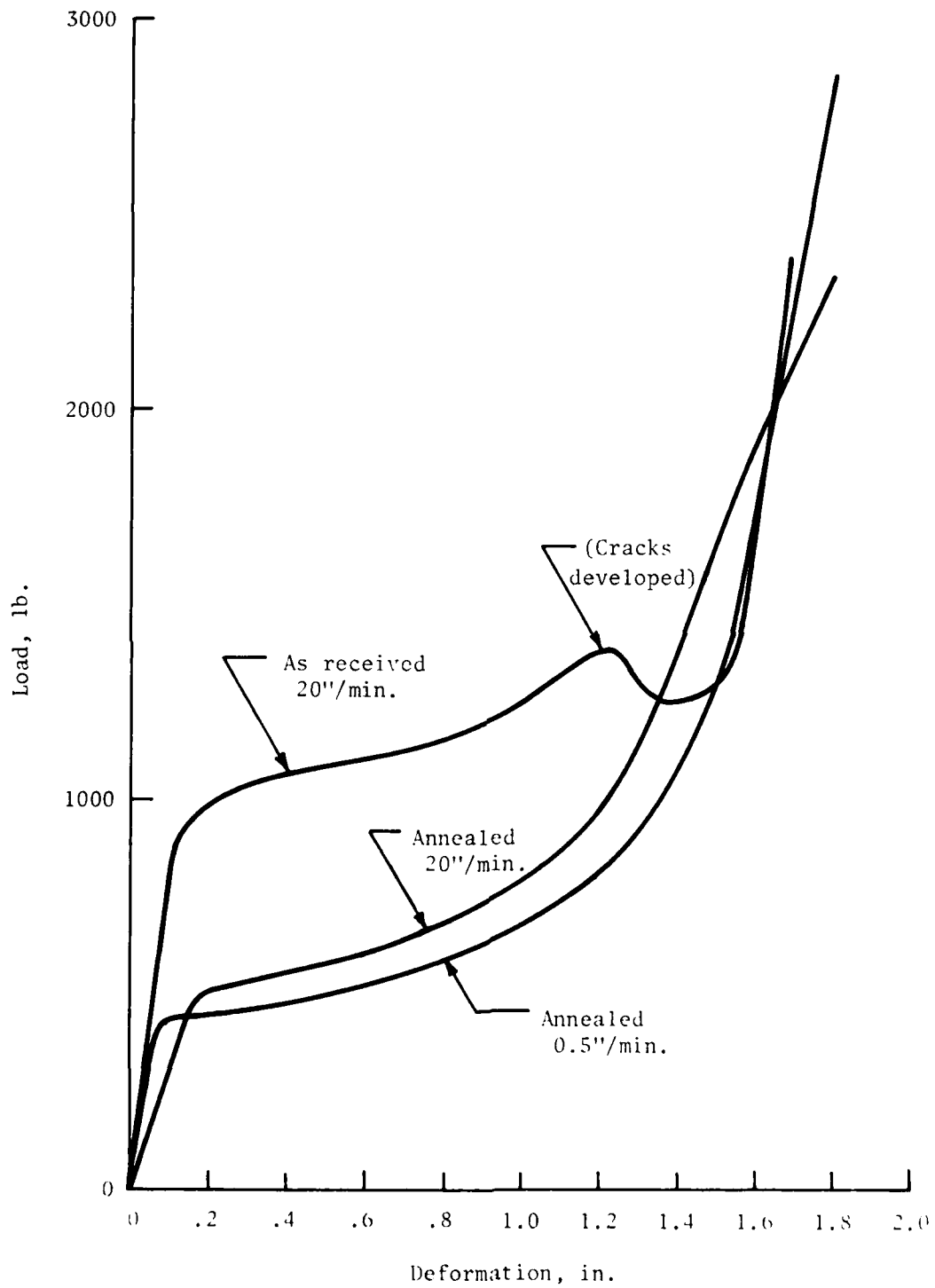


Figure 8. Load vs. deformation for a 2" long, side-loaded tube, using Tinius-Olsen machine. (Tube edges cut by tube cutter.)

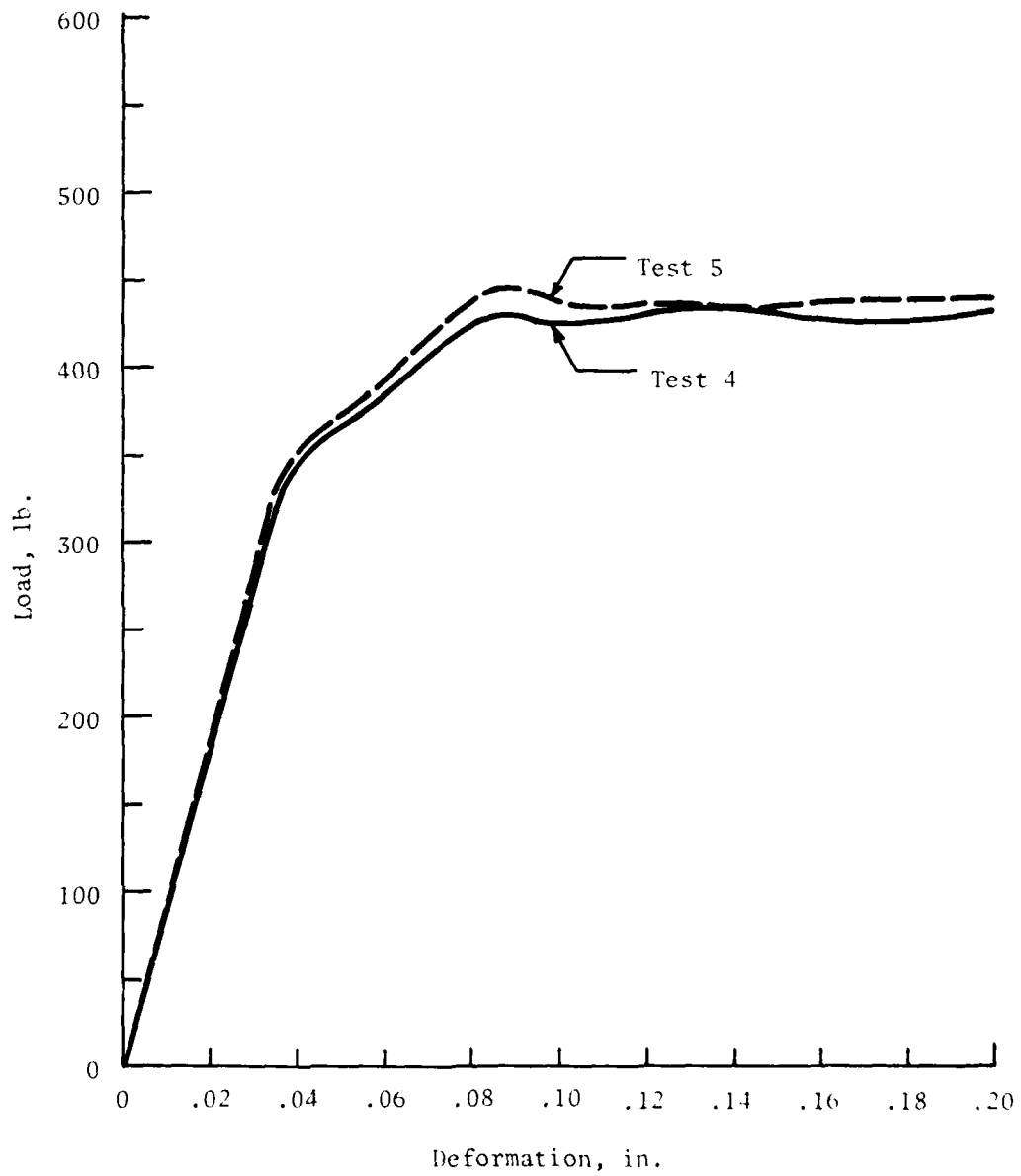


Figure 9. Load vs. deformation for four 1/2" long, annealed, side-loaded tubes using Tinius-Olsen machine.

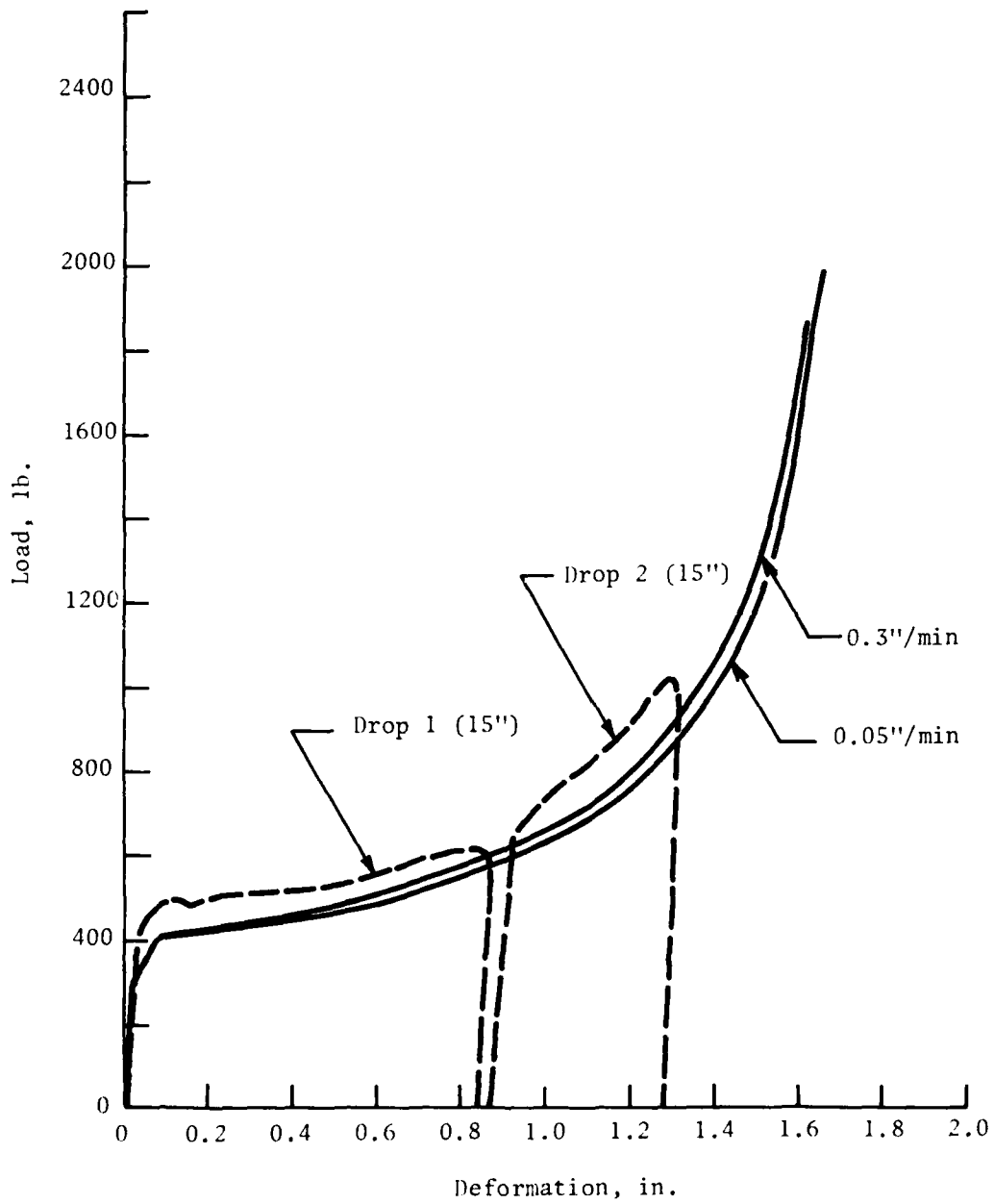


Figure 10. Load vs. deformation for annealed, side-loaded tubes using Tinius-Olsen and shock machines.

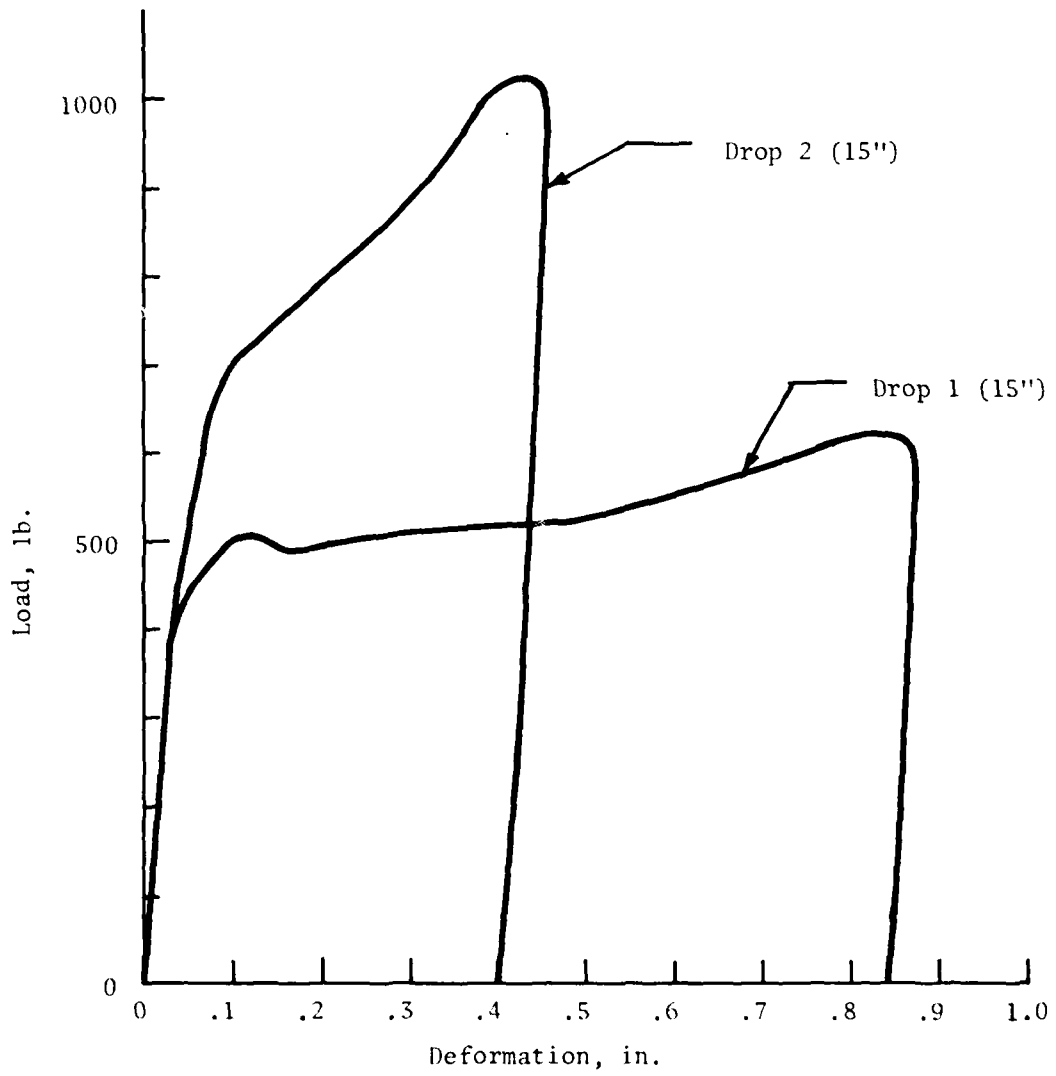


Figure 11. Load vs. deformation for annealed, side-loaded tubes for two successive 15" drops.

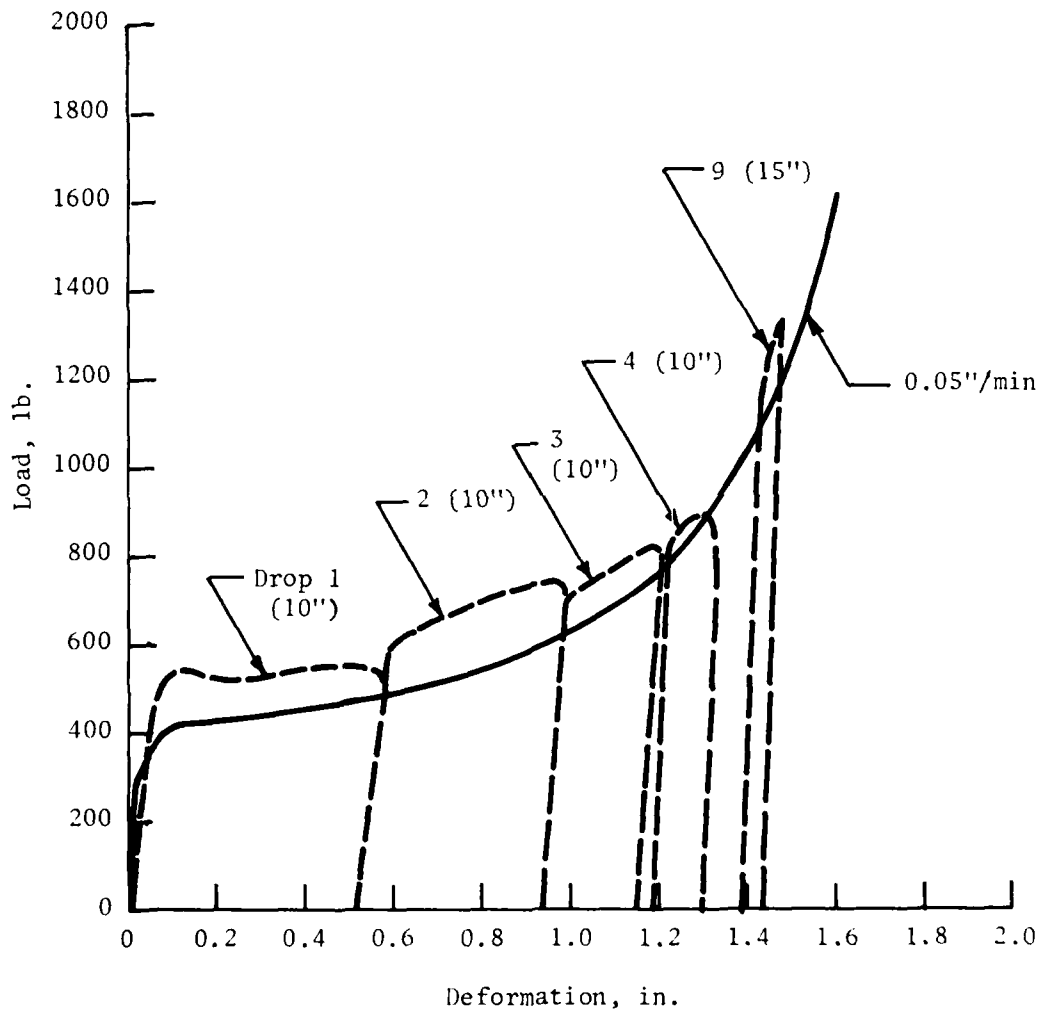


Figure 12. Load vs. deformation for successive drops 1, 2, 3, 4, & 9 compared with quasistatic curve, for side-loaded tubes.

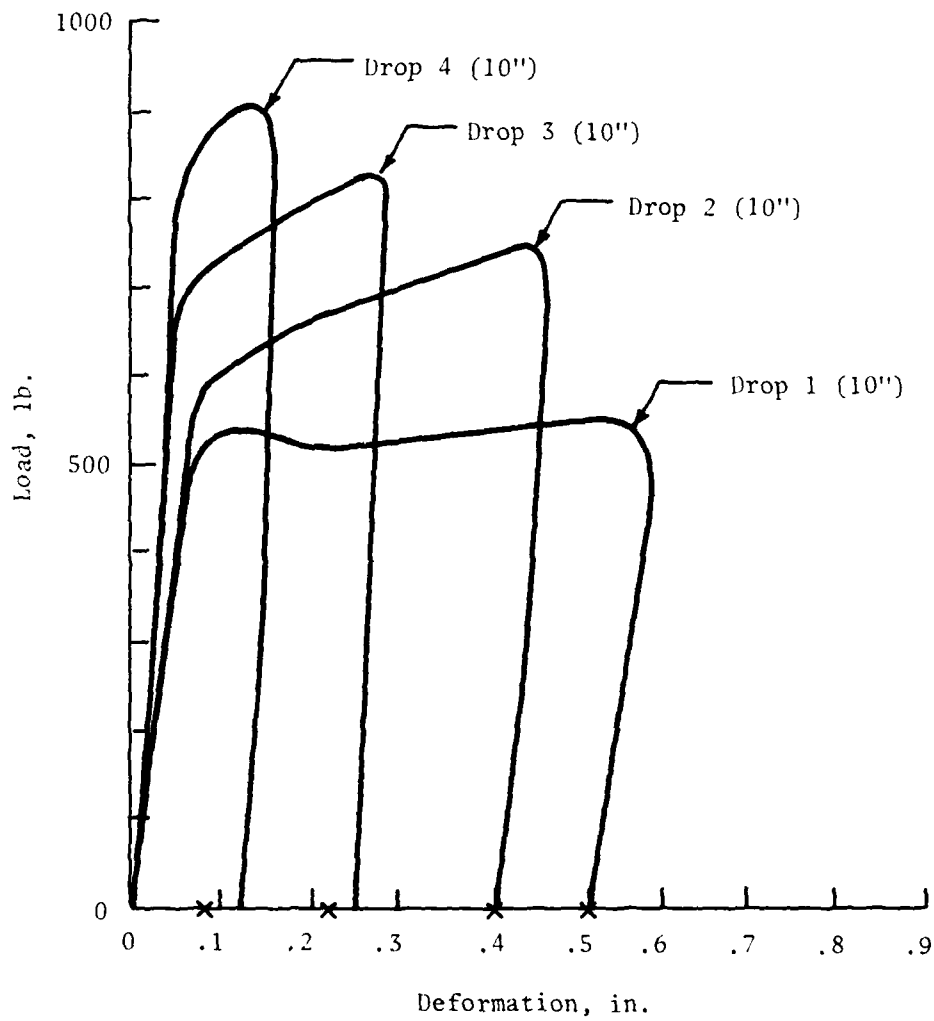


Figure 13. Load vs. deformation for successive drops 1, 2, 3, 4 for side-loaded tubes.

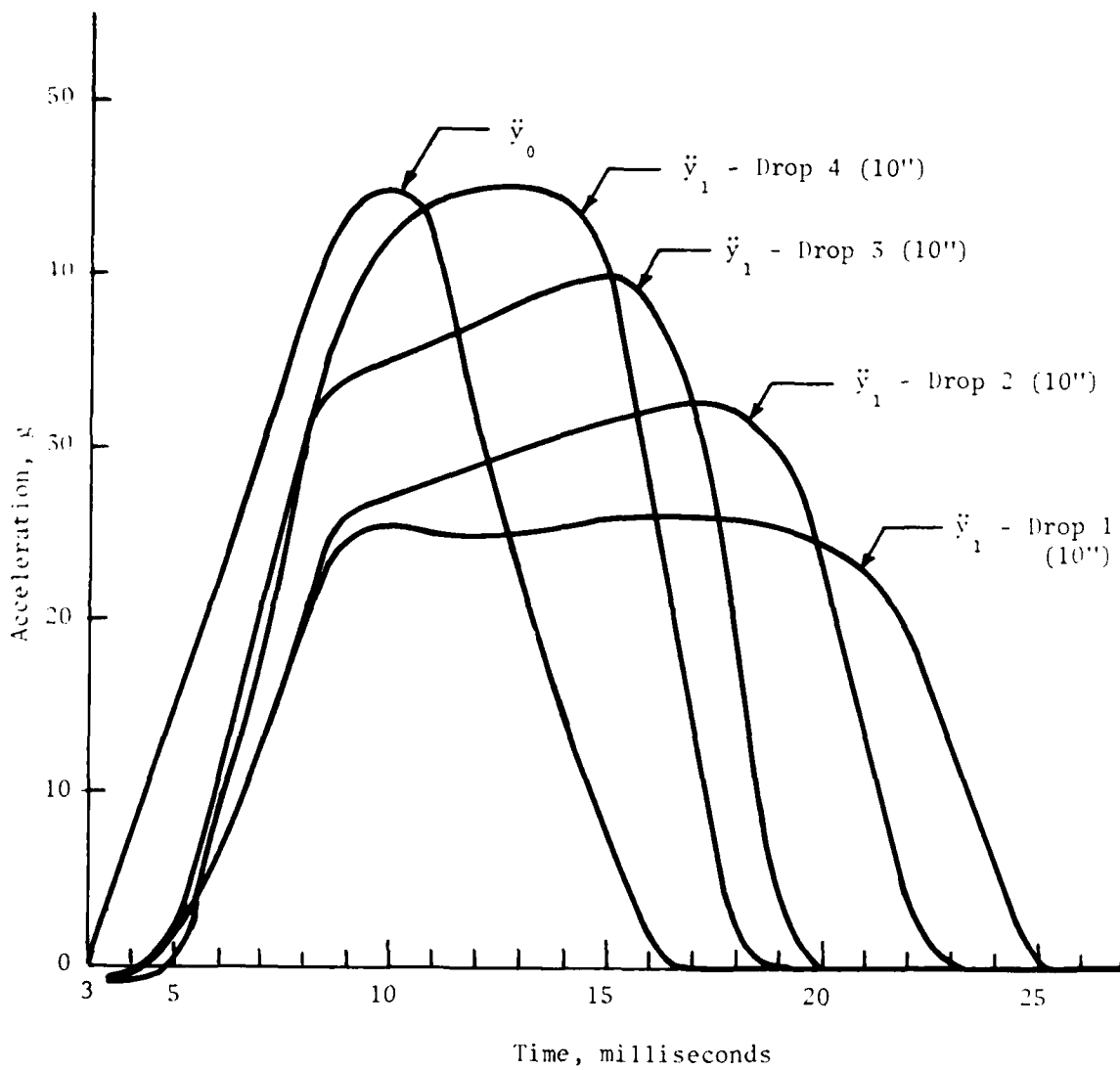


Figure 14. Input acceleration \ddot{y}_0 and transmitted acceleration \ddot{y}_1 versus time, drops 1, 2, 3, & 4 using side-loaded tubes.

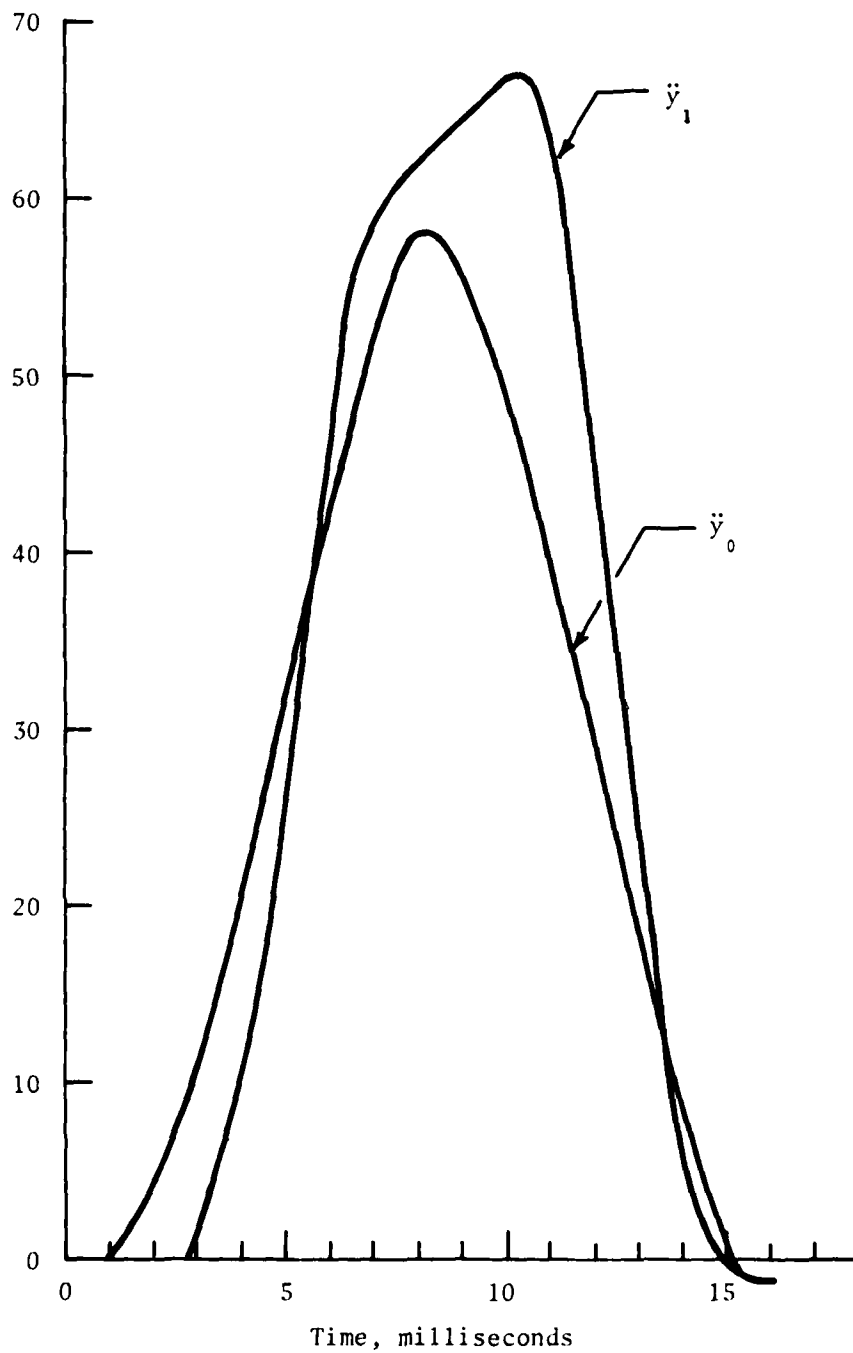


Figure 15. Acceleration vs. time, \ddot{y}_0 and \ddot{y}_1 , for drop 9 using side-loaded tubes in machine-snobber configuration.

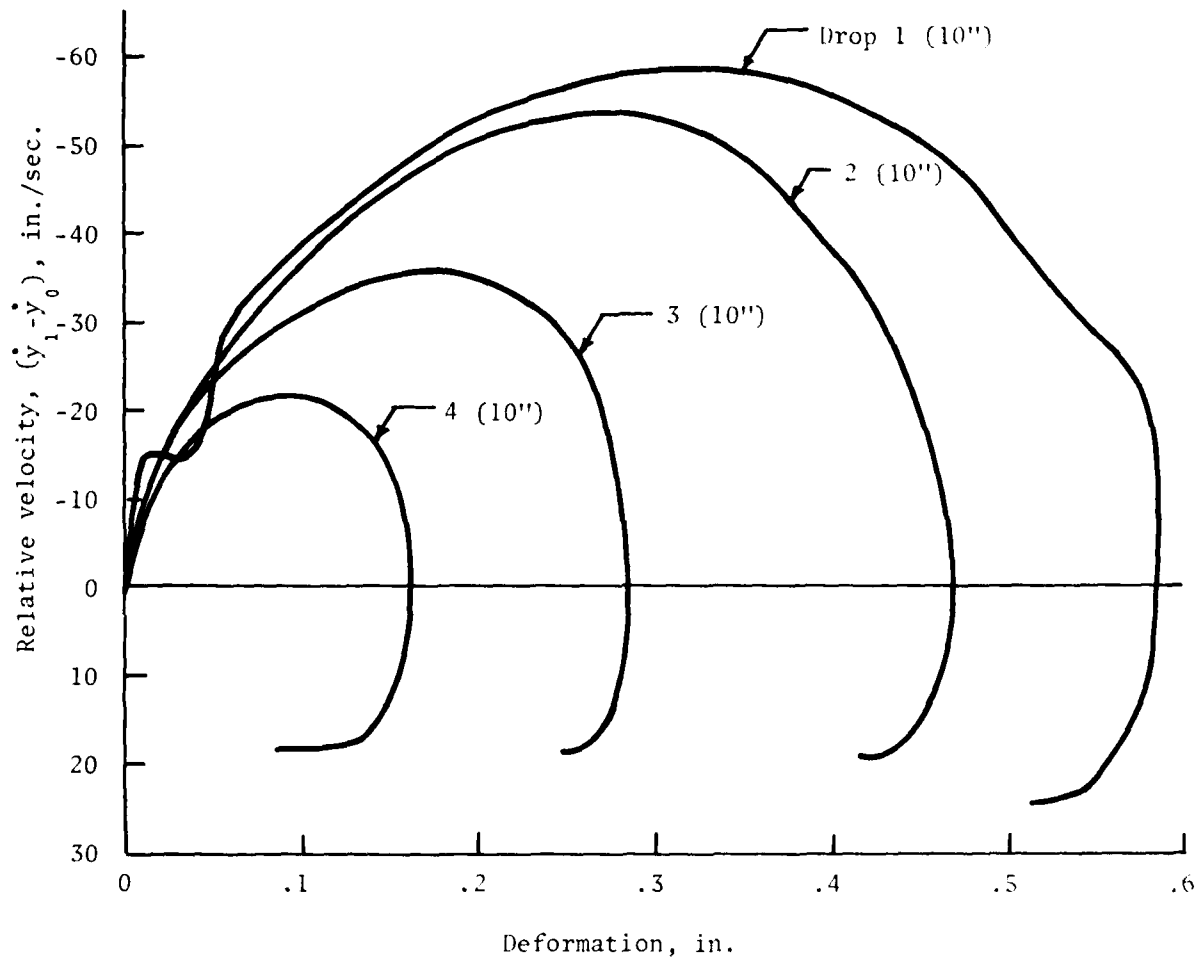


Figure 16. Relative velocity $(\dot{y}_1 - \dot{y}_0)$ vs. deformation for drops 1, 2, 3, & 4 for side-loaded tubes.

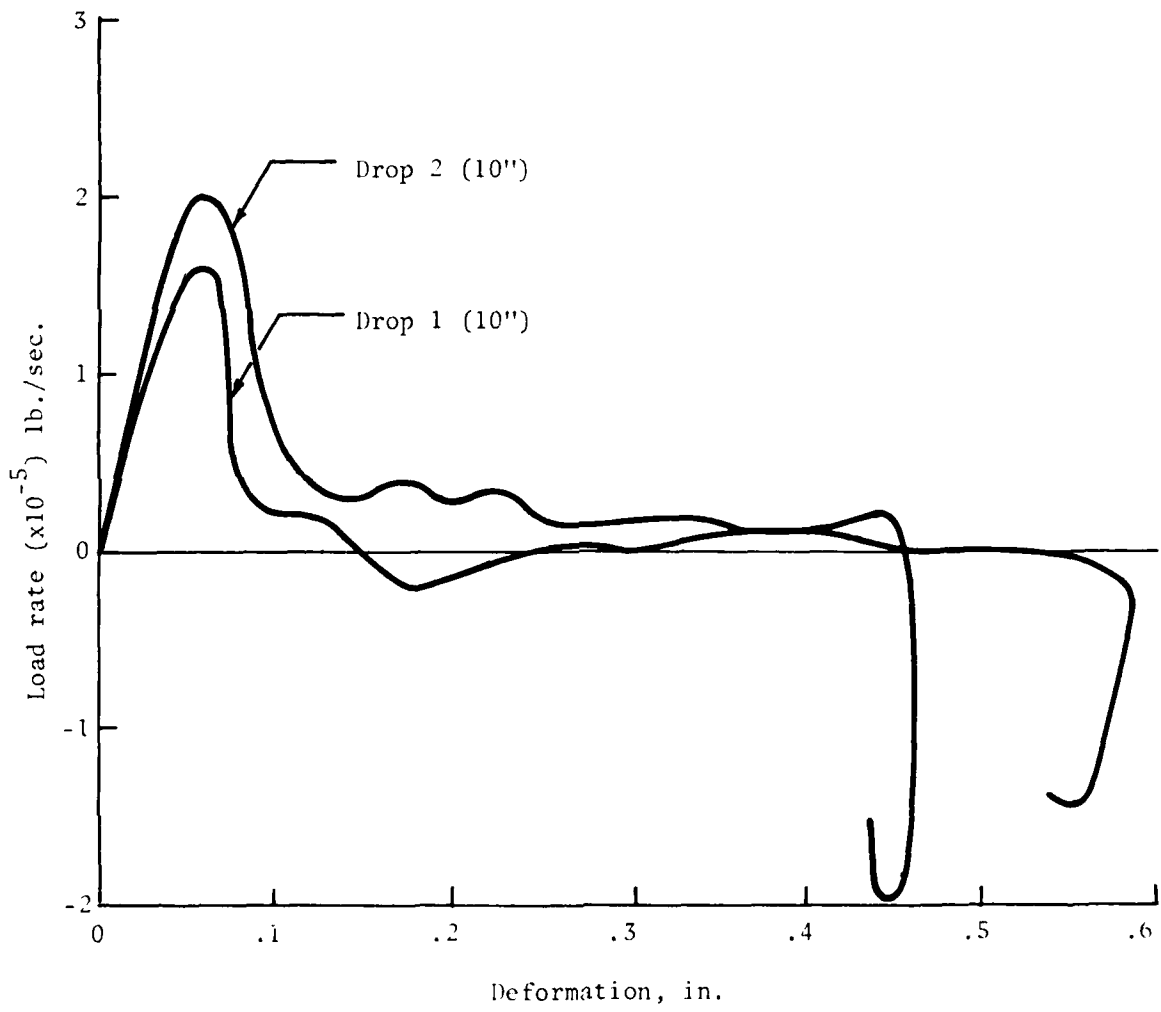


Figure 17. Load rate vs. deformation for 10" drops 1 & 2, for side-loaded tubes.

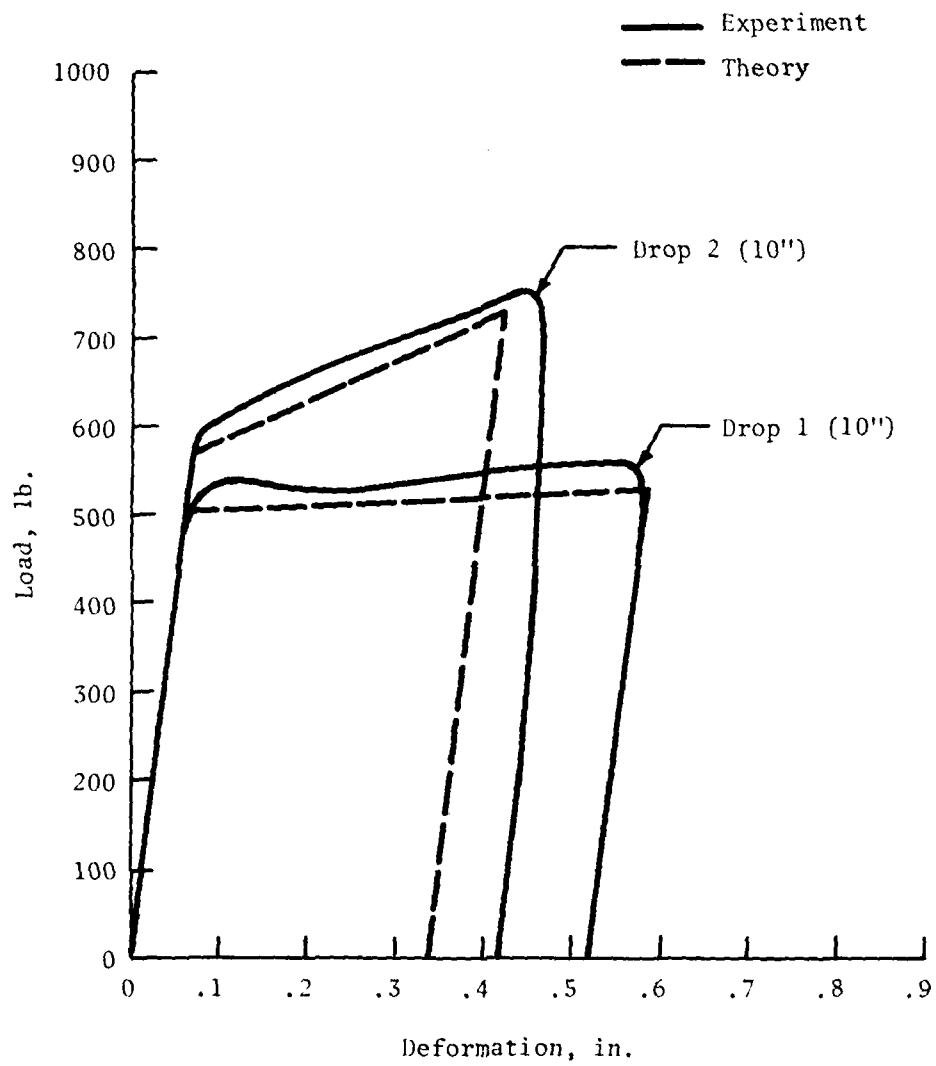


Figure 18. Theoretical and experimental load-deformation curves for 10" drops 1 & 2, for side-loaded tubes.

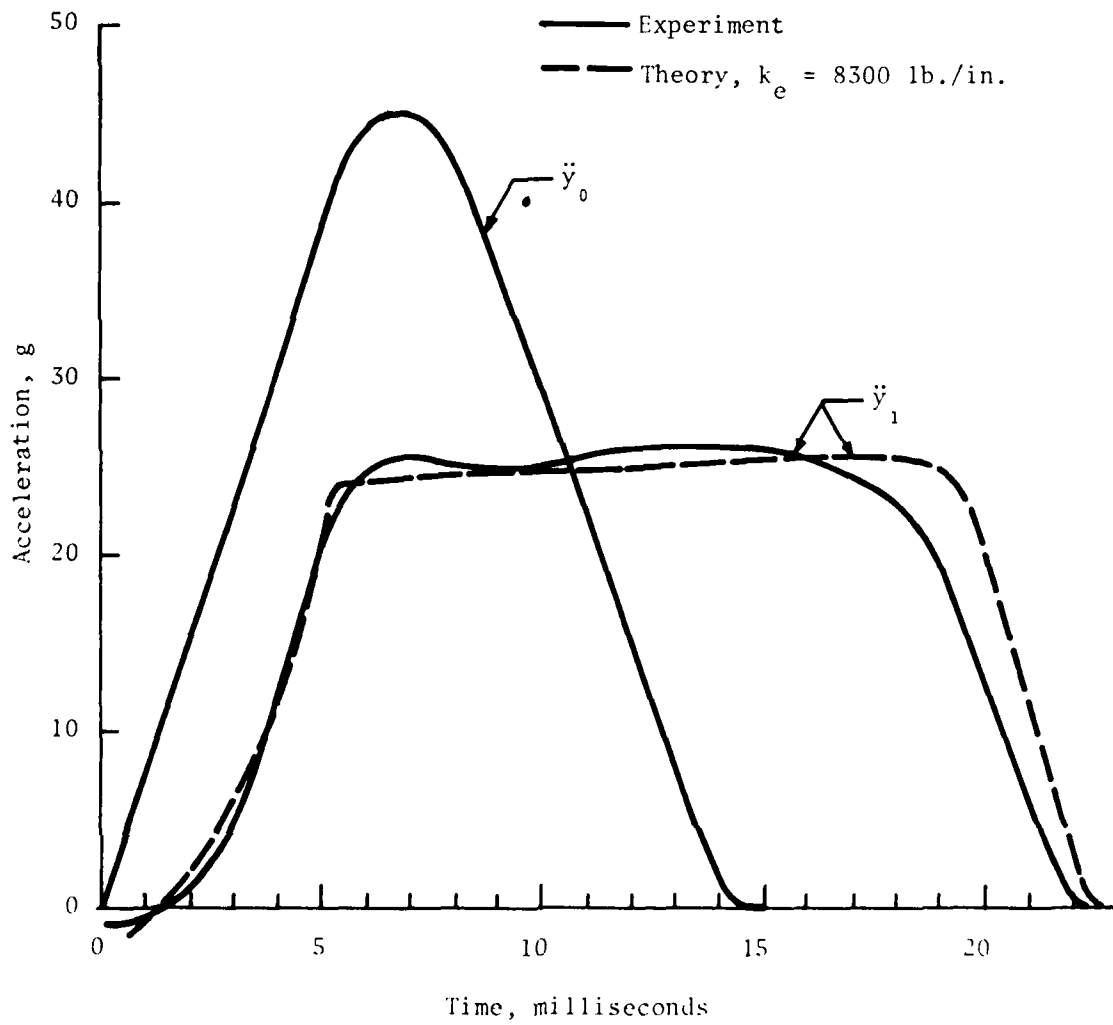


Figure 19. Theoretical and experimental acceleration vs. time; \ddot{y}_1 , for 10' drop 1, for side-loaded tubes.

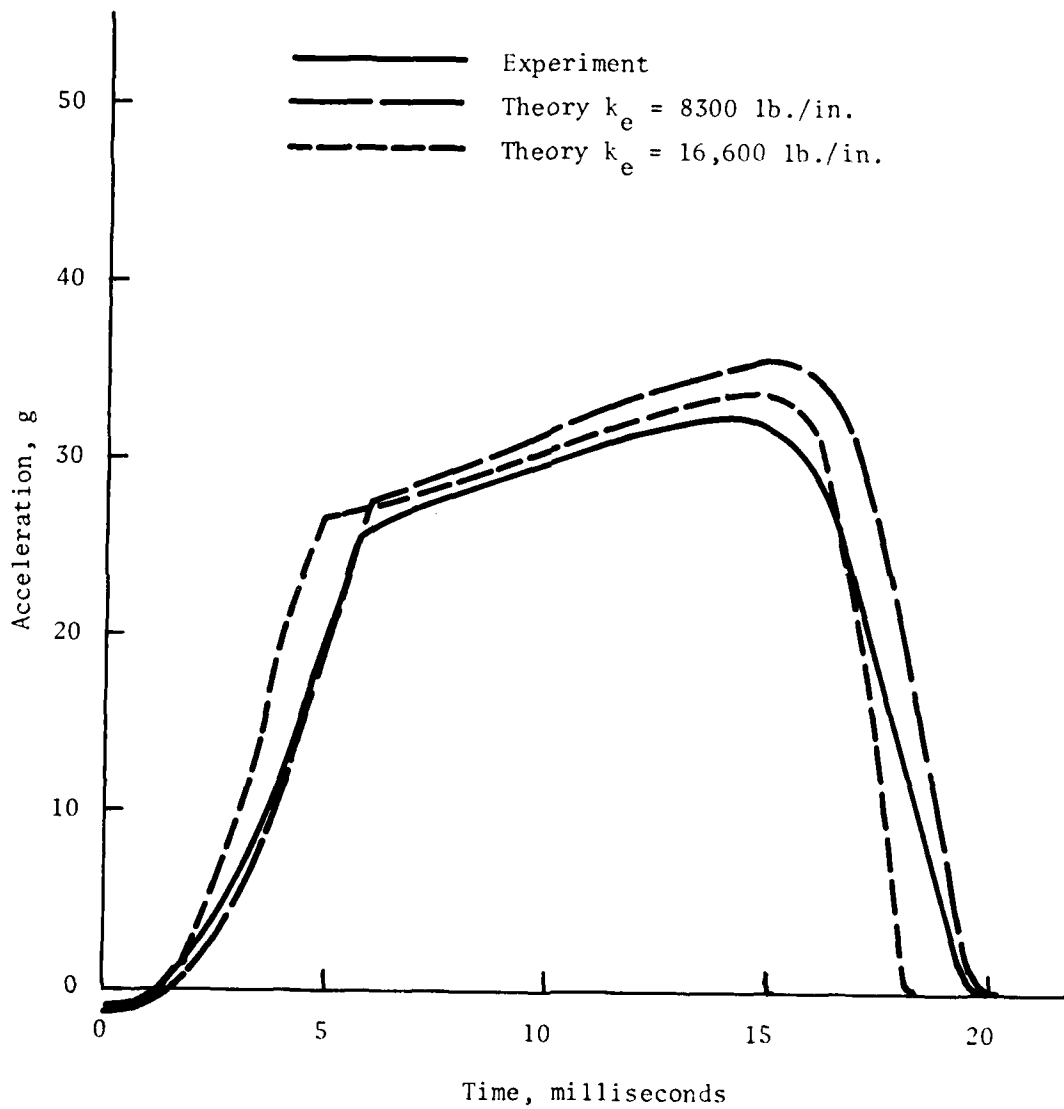


Figure 20. Theoretical and experimental acceleration vs. time; \ddot{y}_1 , for 10" drop 2, for side-loaded tubes.

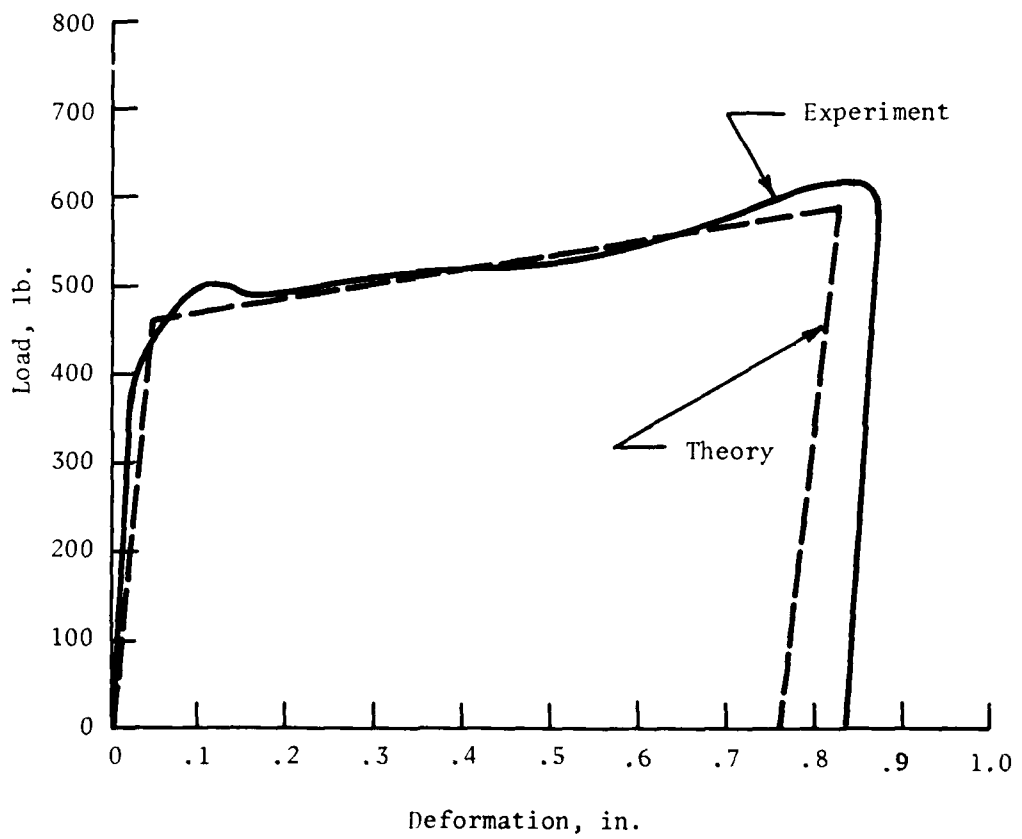


Figure 21. Theoretical and experimental load-deformation curves for 15" drop 1, for side-loaded tubes.

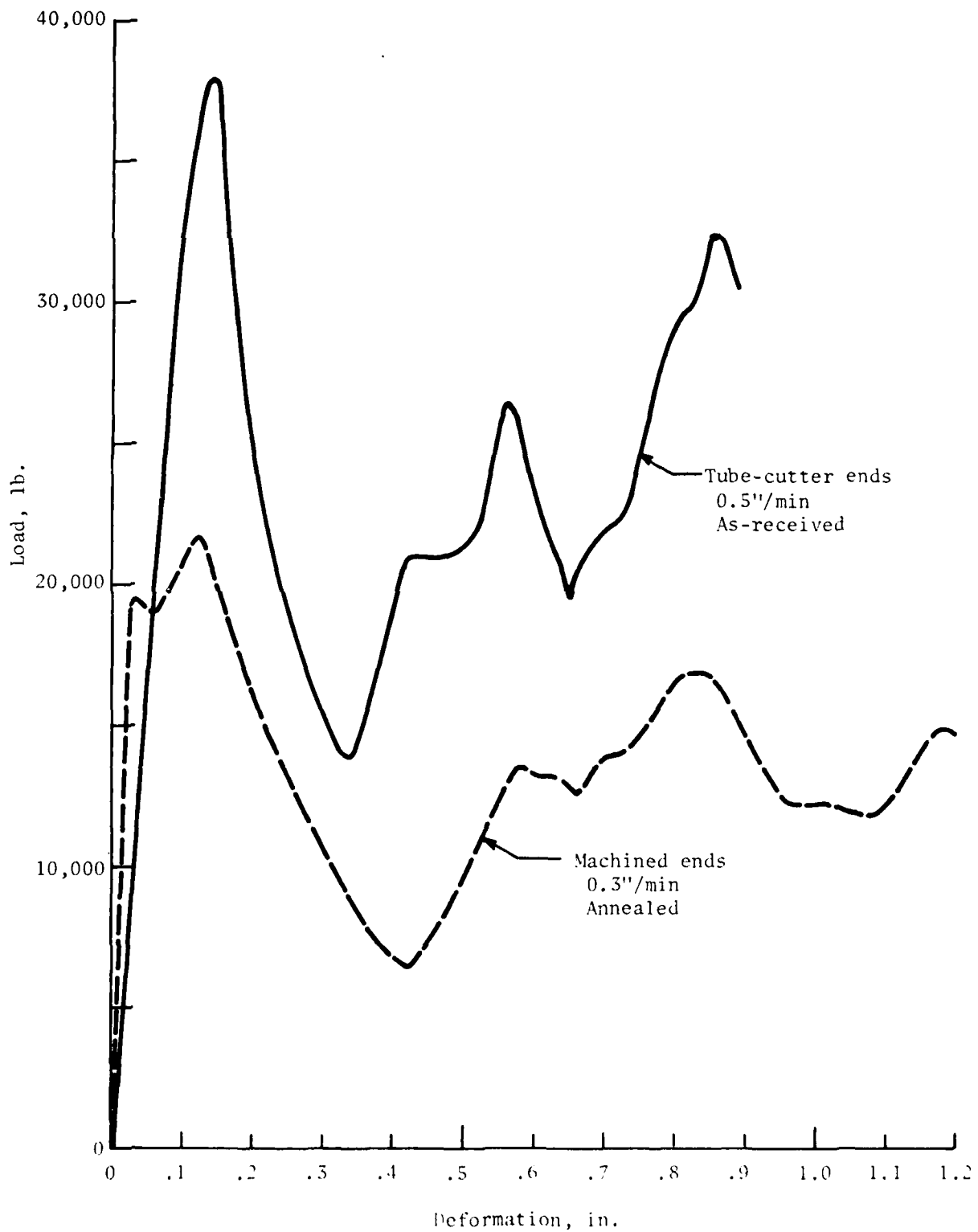


Figure 22. Experimental load versus deformation for as-received and annealed tubes loaded axially.

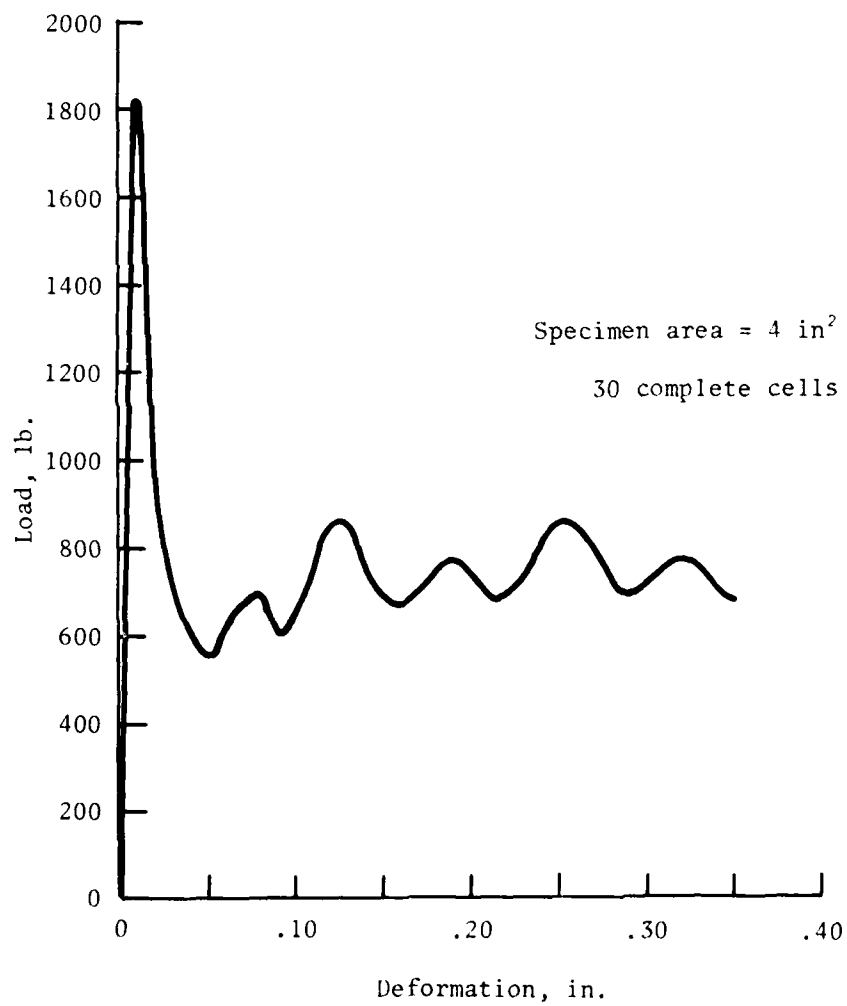


Figure 23. Experimental load versus deformation for aluminum honeycomb.

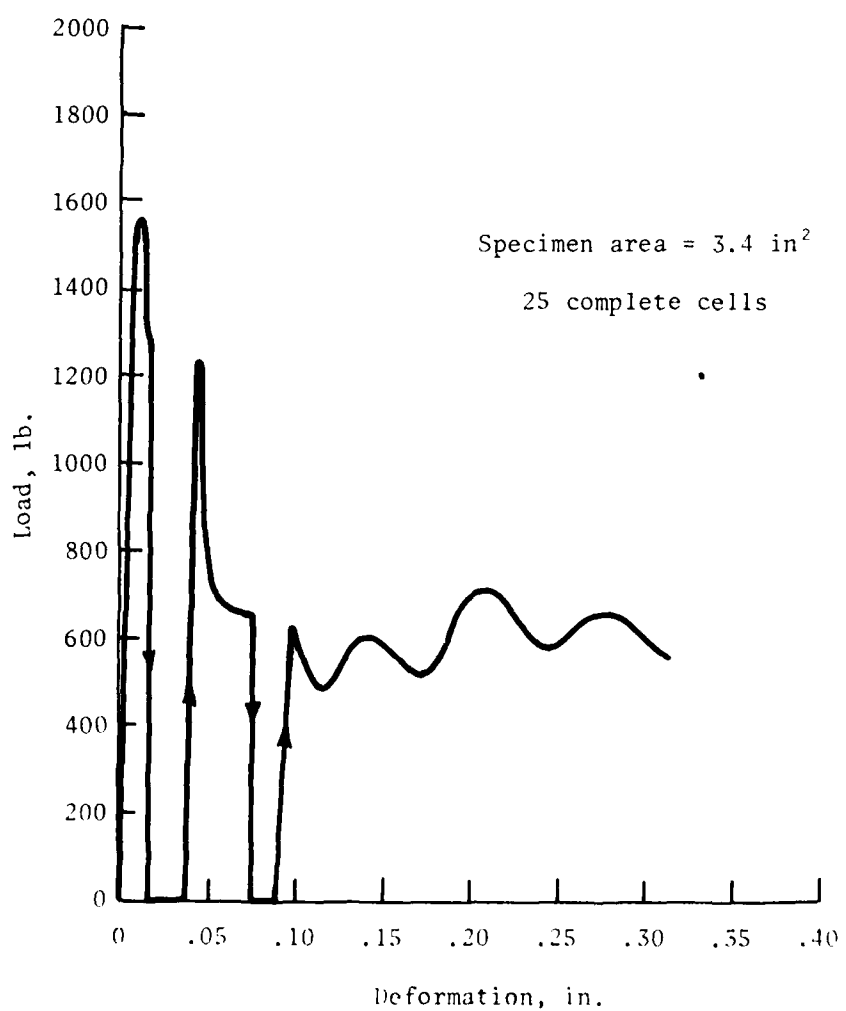


Figure 24. Experimental load versus deformation for aluminum honeycomb during static loading and unloading.

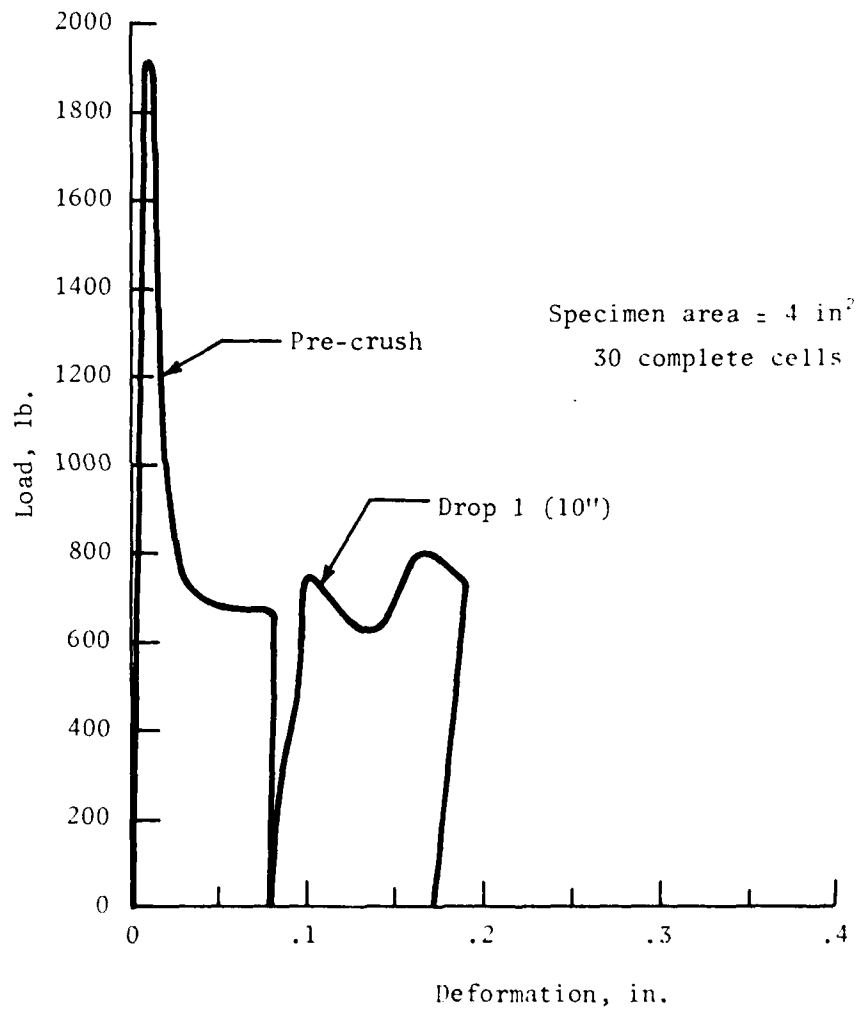


Figure 25. Experimental load versus deformation for aluminum honeycomb for static pre-crush and then 10" drop 1.

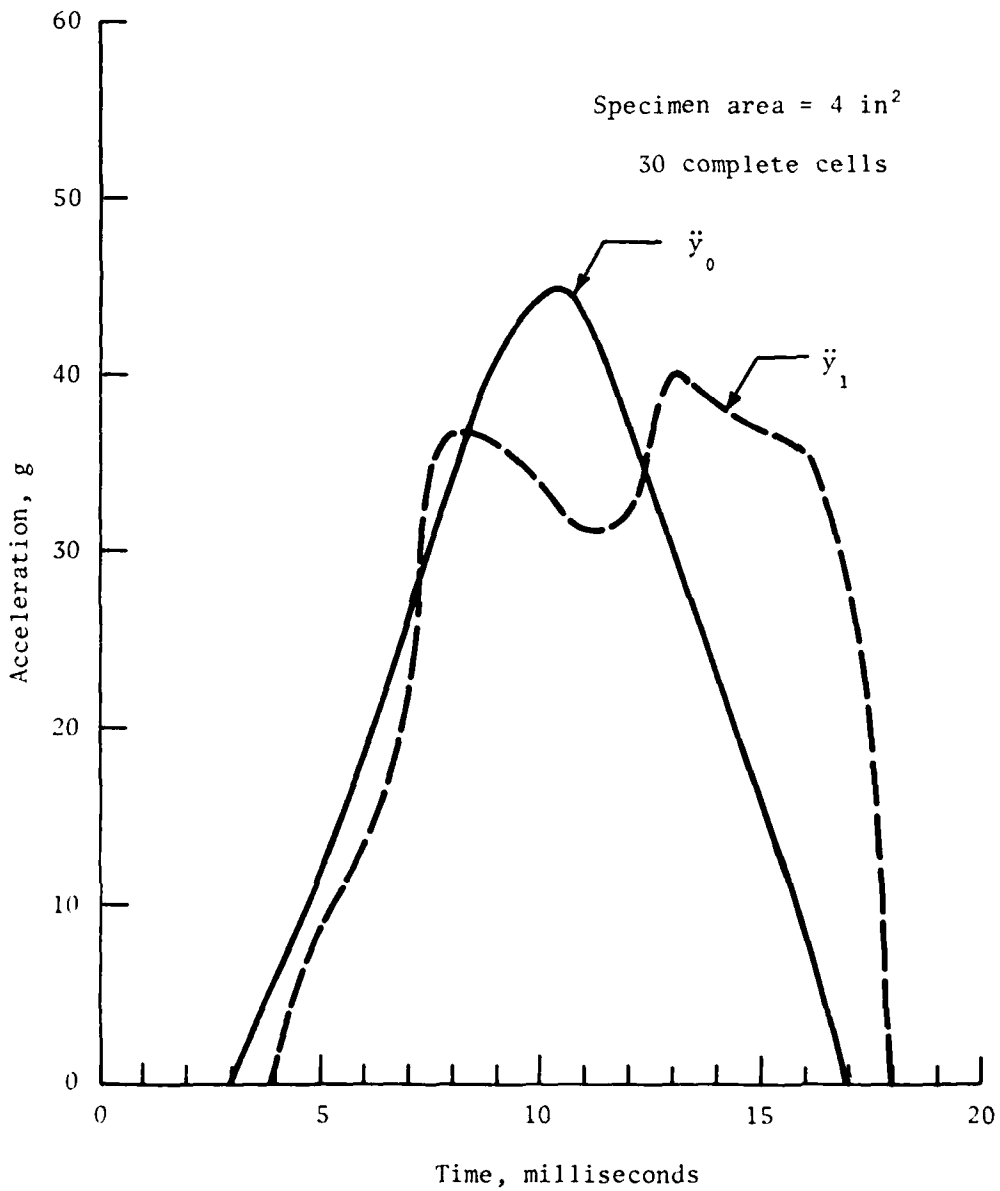


Figure 26. Experimental accelerations, \ddot{y}_0 & \ddot{y}_1 , versus time for aluminum honeycomb for 10" drop 1 after a static pre-crush.

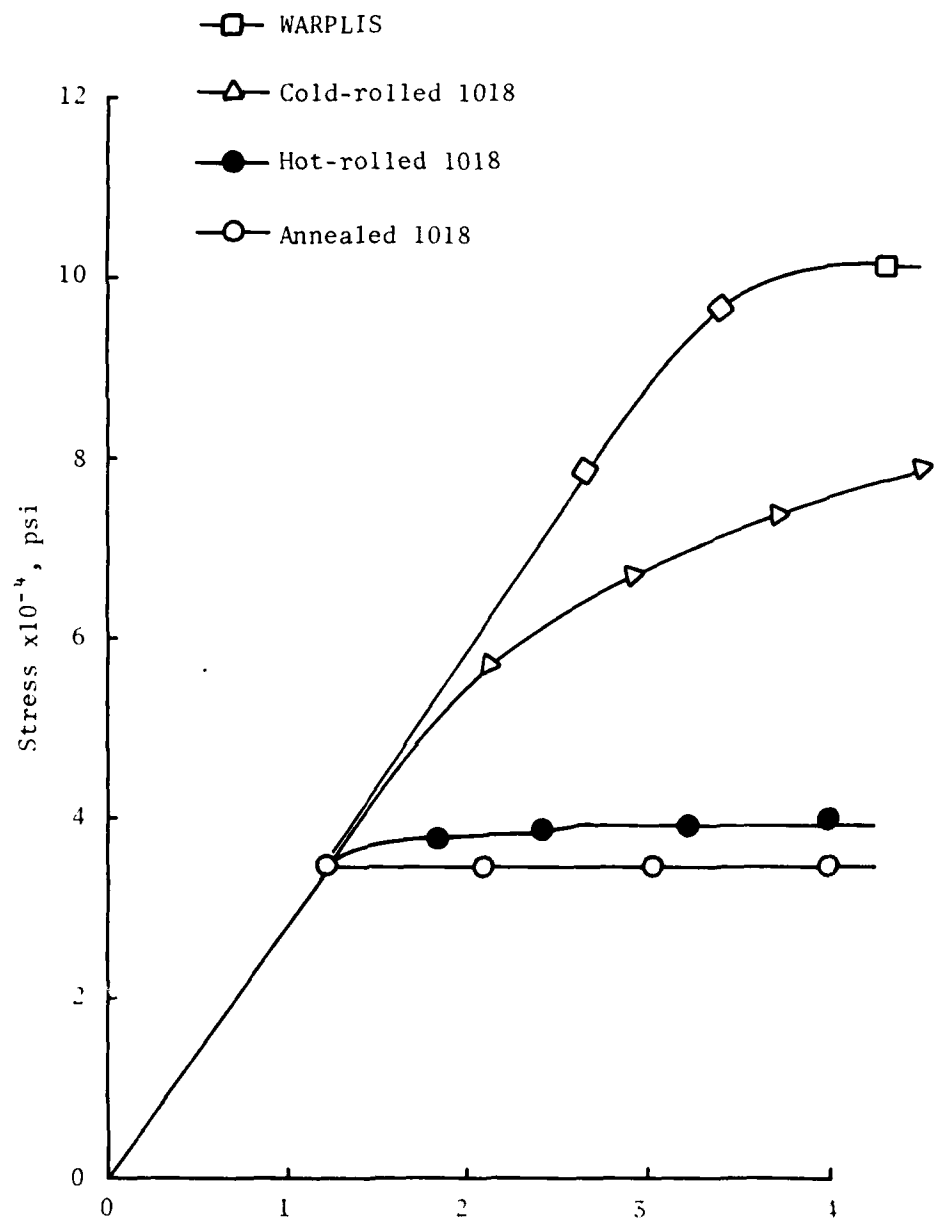


Figure 27. Static stress-strain curves for various steels

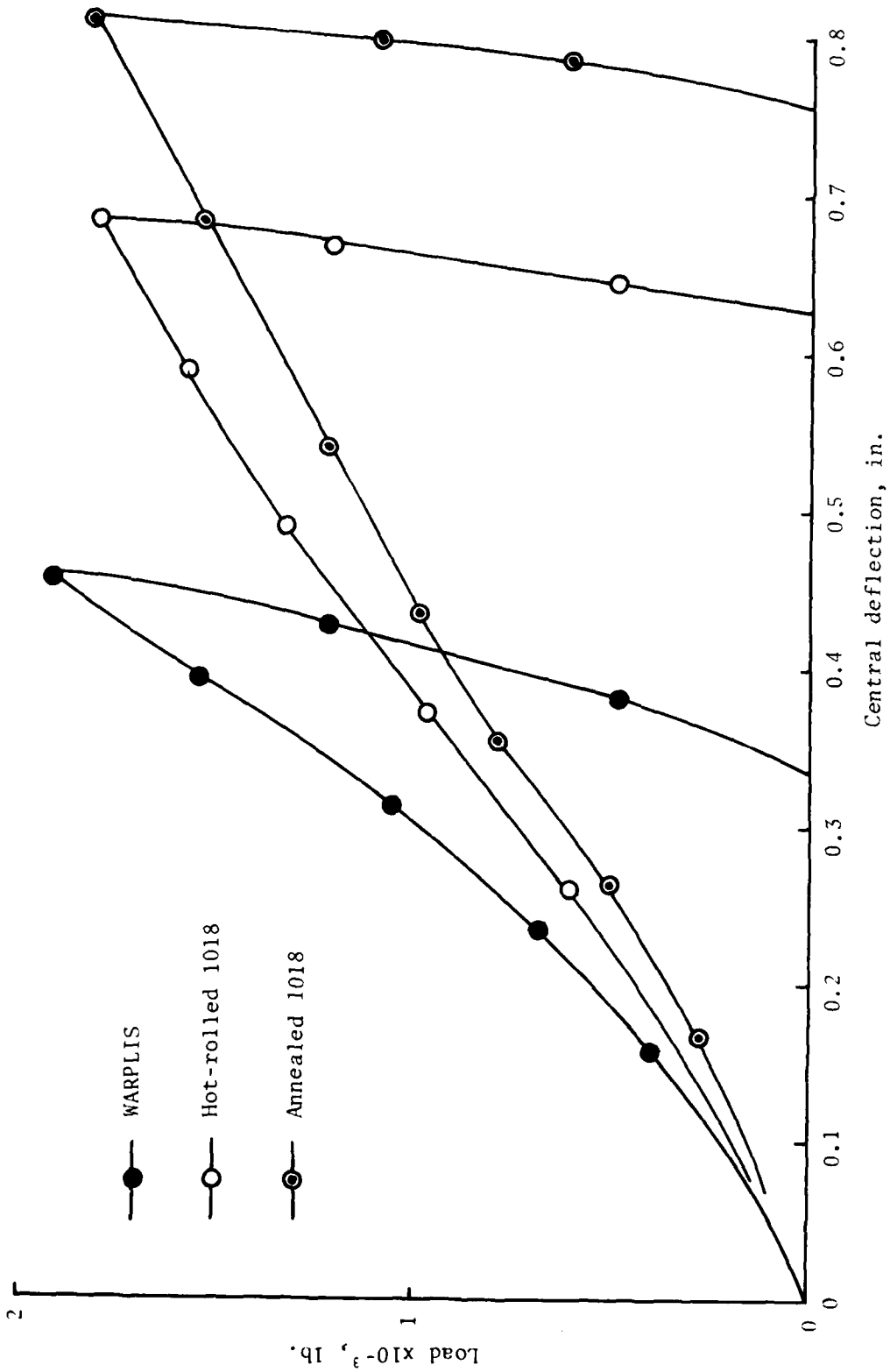


Figure 28. Static load versus central deflection curves for various steel beams.

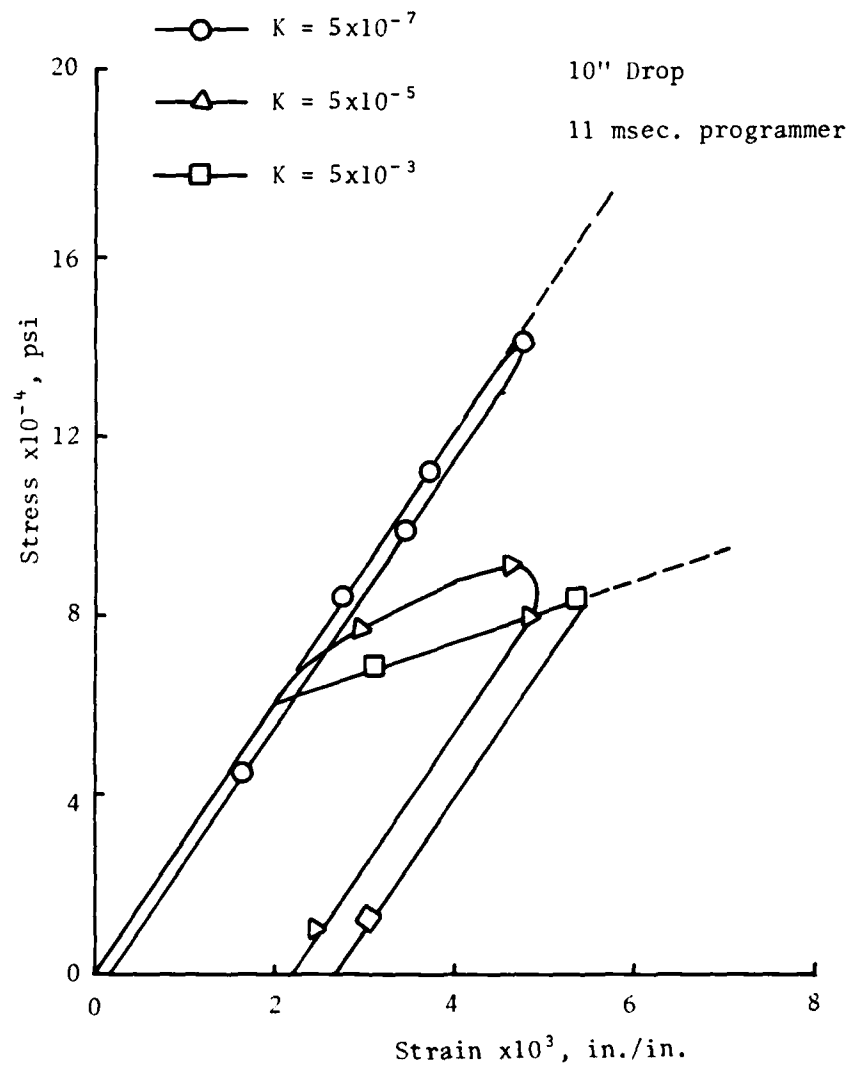


Figure 29. Theoretical dynamic stress-strain for WARPLIS.

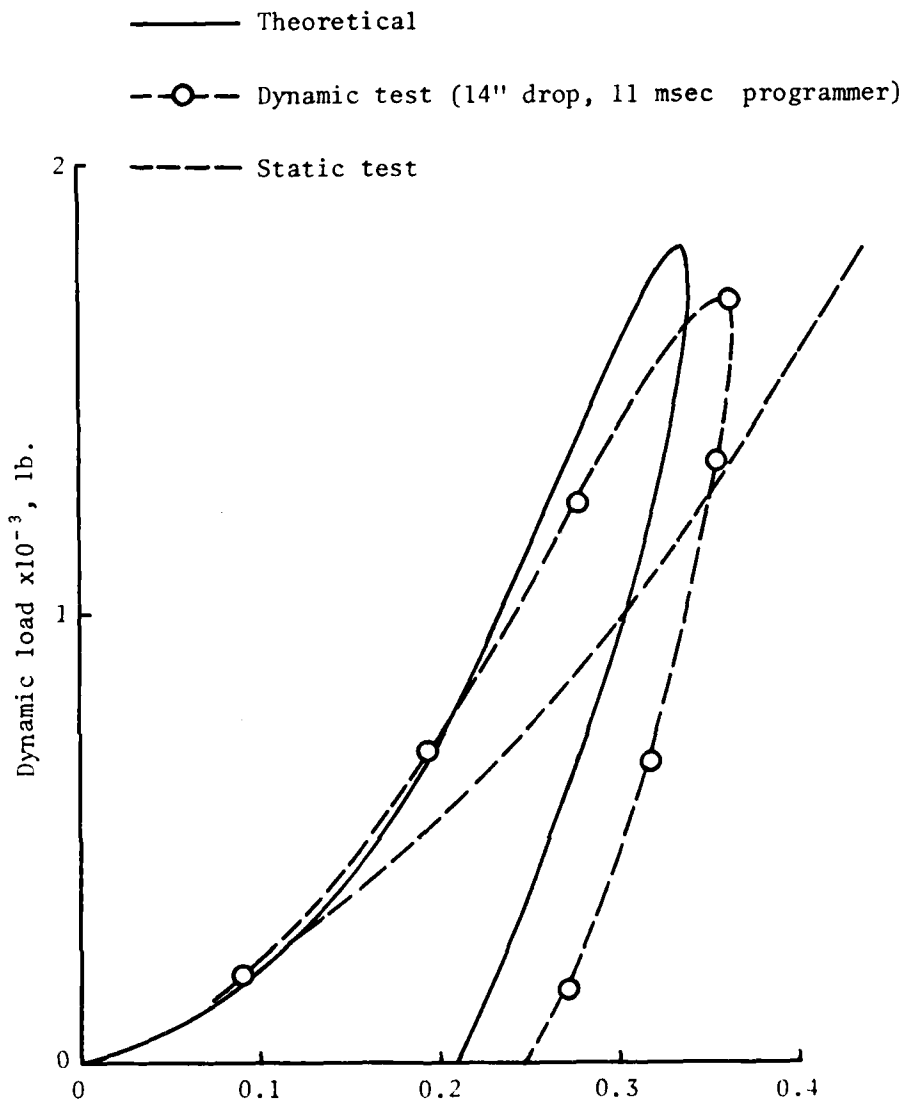


Figure 30. Load vs. central deflection for WARPLIS, dynamic and static loading.

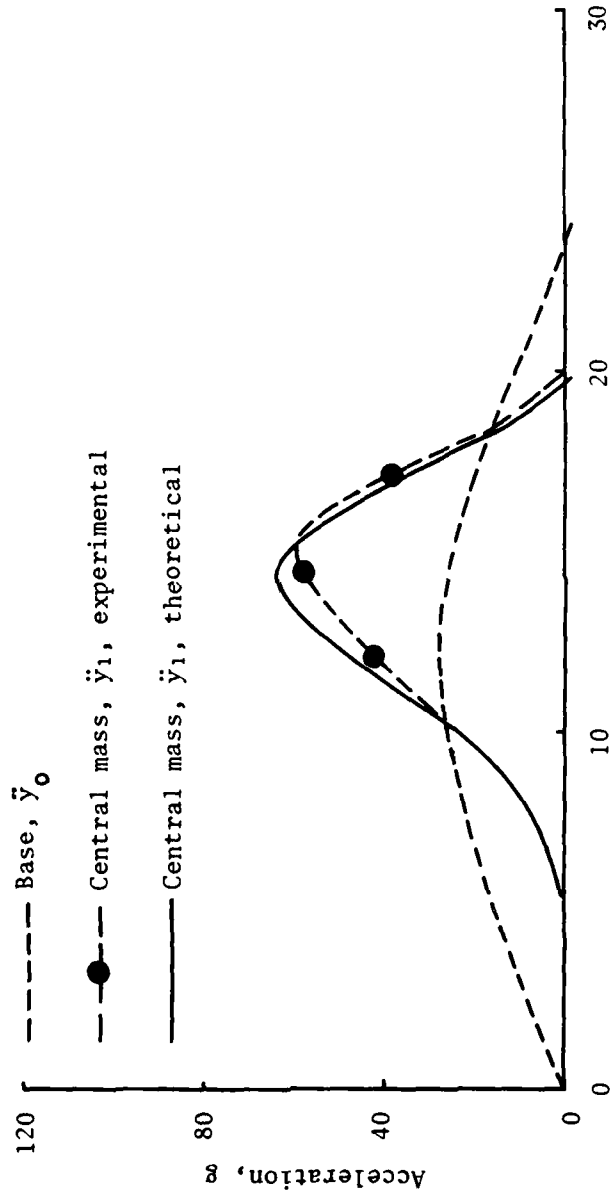


Figure 31. Acceleration-time comparisons for WARPLIS, 10 inch drop, 20 msec programmer

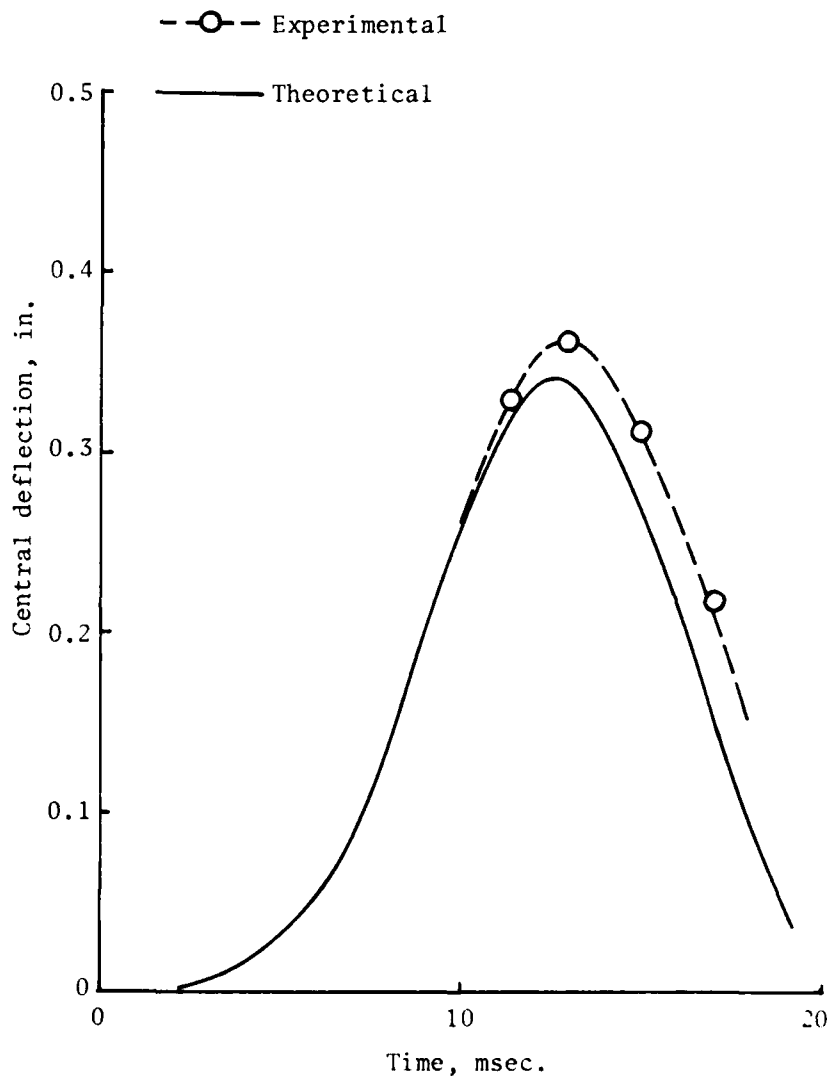


Figure 32. Central deflection vs. time for WARPLIS, 14 inch drop, 11 msec programmer

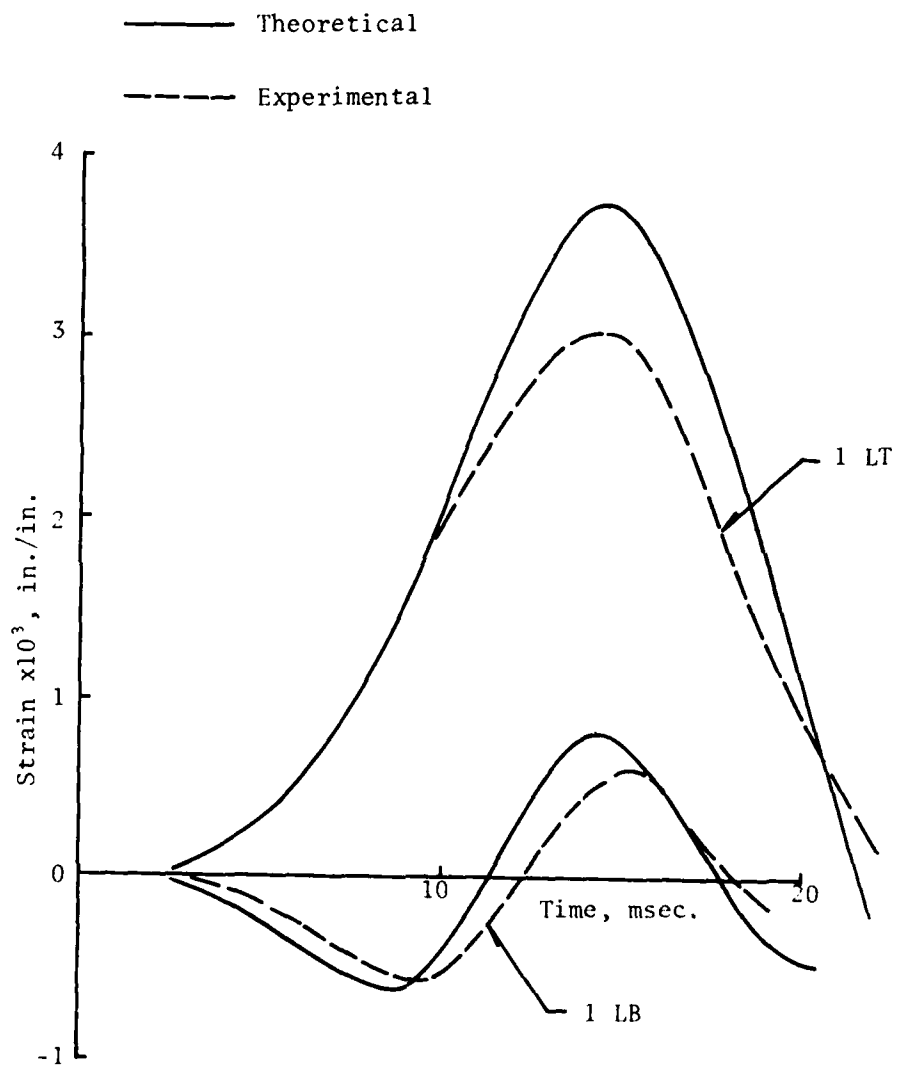


Figure 33. Strain-time comparisons for WARPLIS, 10 inch drop, 20 msec programmer

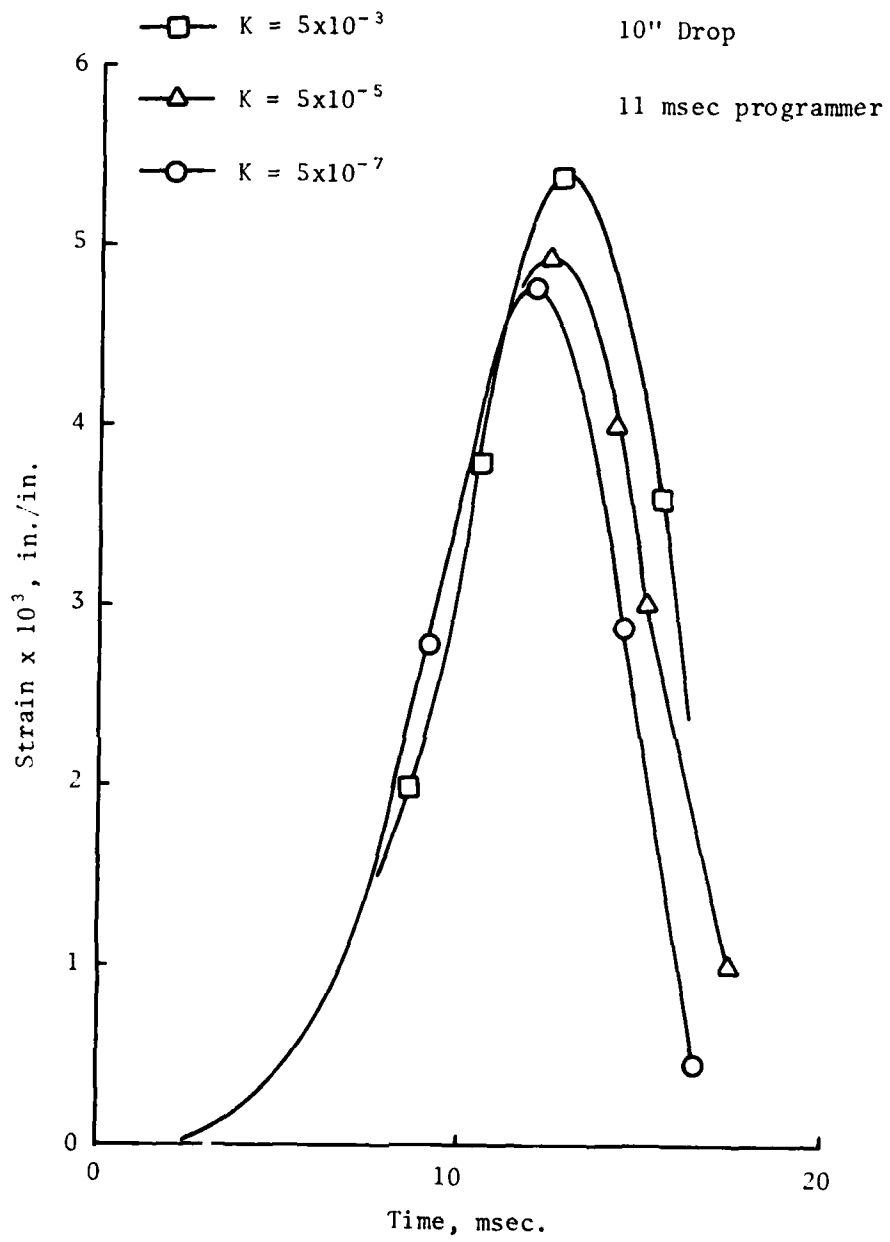


Figure 34. Theoretical strain-time for WARPLIS

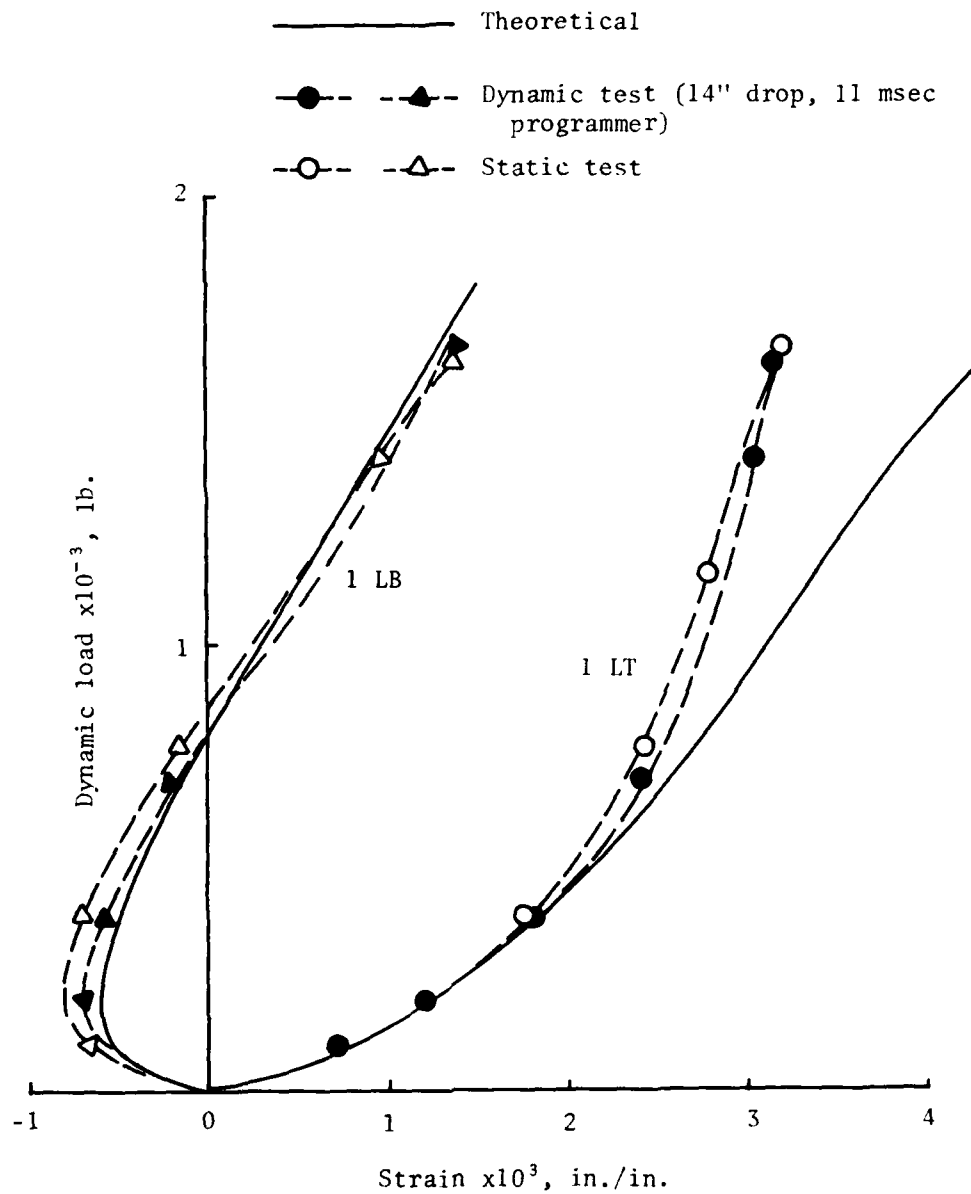


Figure 35. Dynamic load-strain comparisons for WARPLIS, 14 inch drop, 11 msec programmer

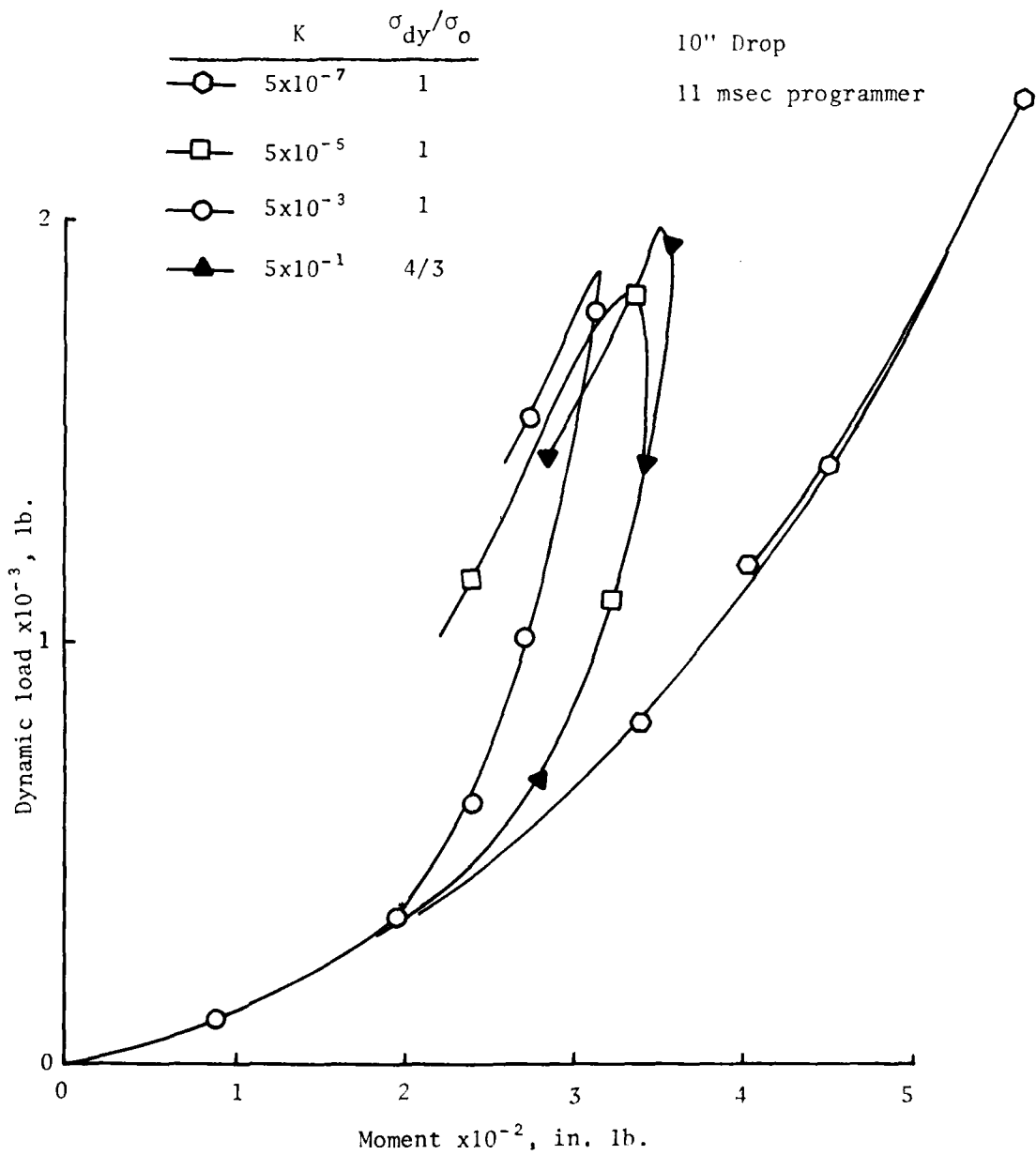


Figure 36. Theoretical dynamic load vs. moment at support for WARPLIS beam.

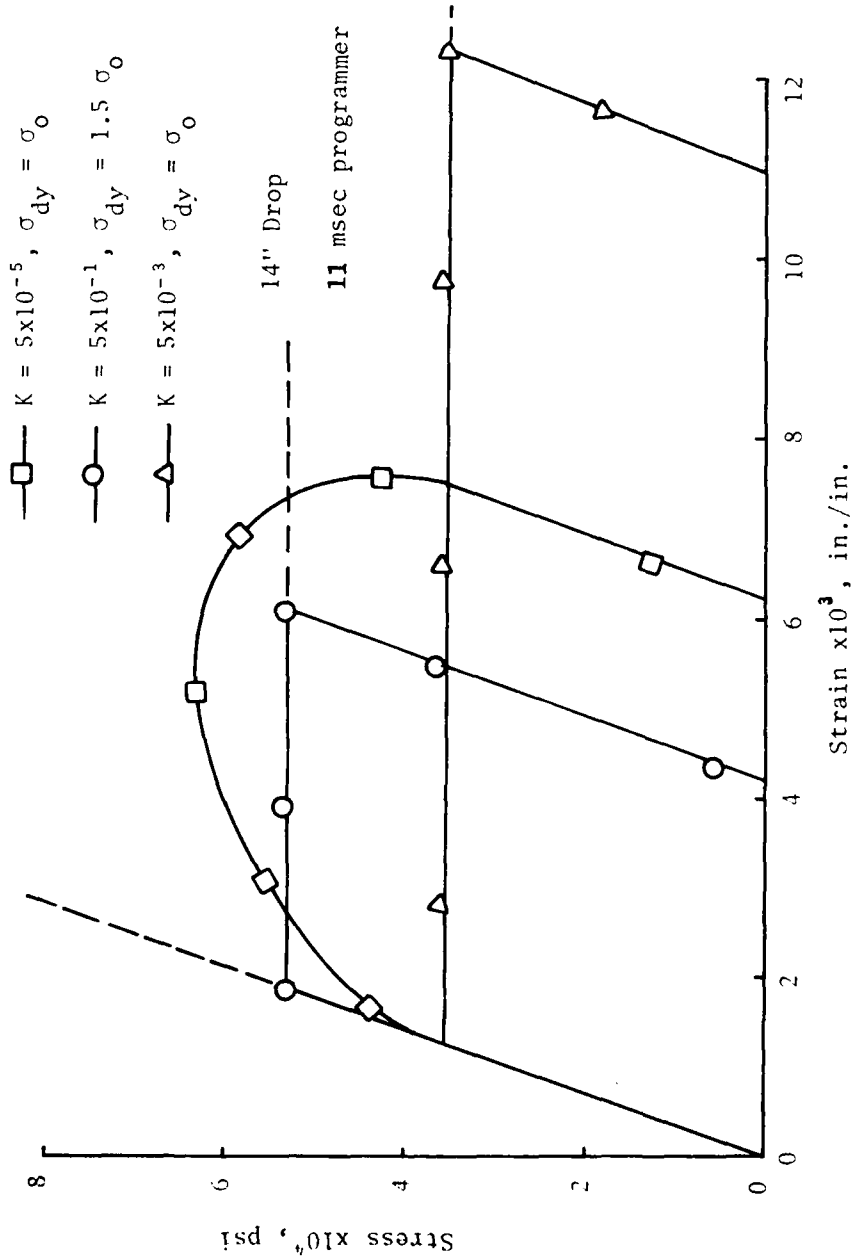


Figure 37. Theoretical dynamic stress-strain relations for annealed 1018 steel

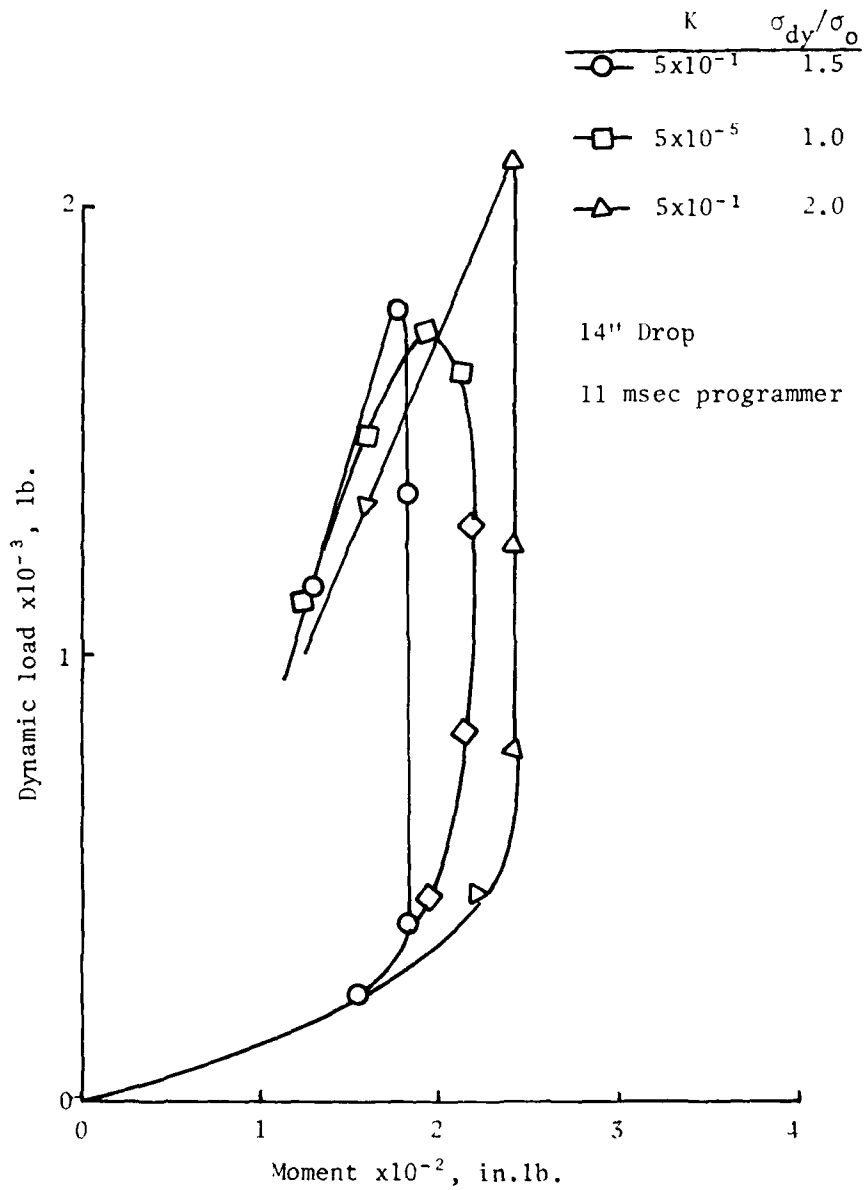


Figure 38. Theoretical dynamic load vs. moment at support for annealed 1018

REFERENCES

1. Stricklin, J. A. and Saczalski, K. J., Constitutive Equations in Viscoplasticity: Computational and Engineering Aspects, ASME Applied Mechanics Division, Vol. 20, 1976.
2. Hecker, S. S., "Experimental Studies of Yield Phenomena in Biaxially Loaded Metals," Reference [1], pp. 1-33.
3. Lindholm, U.S., "High Strain Rate Testing," in Techniques of Metals Research, Vol. V, Bunshah, R. F., Ed., Interscience, N. Y., pp. 199-271, 1971.
4. Cowper, G. R. and Symonds, P. S., "Strain Hardening and Strain Rate Effects in the Impact Loading of Cantilever Beams," Technical Report No. 28, Brown University, 1957.
5. Manjoine, M. J., "Influence of Rate of Strain and Temperature on Yield Stress of Mild Steel," J. Appl. Mech., 11, 211, 1944.
6. Parkes, E. W., "The Permanent Deformation of an Encastre Beam Struck Transversely at Any Point in its Span," Proc. of the Inst. of Civil Eng., Vol. 10, pp. 277-304, 1958.
7. Belsheim, R. O., "Delayed Yield Time Effects in Mild Steel Under Oscillatory Axial Loads," Trans. ASME, 1957.
8. Vigness, I., Krafft, J. M., and Smith, R. C., "Effect of Loading History Upon the Yield Strength of a Plain Carbon Steel," Proc. Inst. Mech. Engrs., 1957.
9. Malvern, L. E., "The Propagation of Longitudinal Waves of Plastic Deformation in a Bar Exhibiting a Strain Rate Effect," J. Appl. Mech., 18, 203, 1951.
10. Cristescu, N., Bul. Acad. Pol. Sci., XI, 129, 163. See also "A Procedure for Determining the Constitutive Equations for Materials. Both Time-Dependent and Time-Independent Plasticity," Int. J. Solids and Structures, Vol. 8, pp. 511-531, 1972.
11. Perrone, Nicholas, "A Mathematically Tractable Model of Strain Hardening, Rate-sensitive Plastic Flow," J. Appl. Mech., 33, 210-211, 1966.
12. Plass, H. J., Jr., "Theory of Plastic Bending Waves in a Bar of Strain Rate Material," Second Midwestern Conference on Solid Mechanics, pp. 109-134, 1955.
13. Hwang, Chintsun, "Plastic Collapse of Thin Rings," Int. of Aero. Sci., pp. 819-826, Dec. 1953.
14. DeRuntz, J. A., Jr. and Hodge, P. G., Jr., "Crushing of a Tube Between Rigid Plates," Int. of Appl. Mech., pp. 391-395, Sept. 1963.
15. Perrone, N., "On a Simplified Method for Solving Impulsively Loaded Structures of Rate-Sensitive Materials," J. Appl. Mech., 33, 489-493, 1965.
16. Perrone, N., "Thick-Walled Rings for Energy-Absorbing Bridge Rail Systems," Final Report No. FHWZ-RD-73-49, for Federal Highway Administration Offices of Research and Development, Washington, D. C., 20590, December 1972.
17. Thompson, J. N. and Ripperger, E. A., "Cushioning for Aerial Delivery," Shock and Vibration Bulletin No. 30, Part. 3, pp. 261-275, Feb. 1962.

18. McFarland, R. K., Jr., "Hexagonal Cell Structures under Post-Buckling Axial Load," AIAA Journal, Vol. 1, No. 4, pp. 1380-1385, 1963.
19. Lewallen, J. M. and Ripperger, E. A., "Energy-Dissipating Characteristics of Truss-grid Aluminum Honeycomb," Structural Materials Research Lab. Report SMRL RM-5, University of Texas, March 1962.
20. Alexander, J. M., "An Approximate Analysis of the Collapse of Thin Cylindrical Shells under Axial Loading," Quart. J. Mech. & Appl. Math. XIII, 10-14, 1960.
21. Pugsley, A. and Macaulay, M., "The Large-scale Crumpling of Thin Cylindrical Columns," Quart. J. Mech. and Appl. Math. VIII, 1-9, 1960.
22. McGehee, J. R., "Experimental Investigation of Parameters and Materials for Fragmenting Tube Energy Absorbing Process," NASA TN D-3268, 1966.
23. Kroell, C. K., "A Simple, Efficient, One Shot Energy Absorber," Shock and Vibration Bulletin No. 30, Part III, pp. 331-338, February 1962.
24. Shaw, Milton C., "Design for Safety: The Mechanical Fuse," Mechanical Engineering, pp. 23-29, April, 1972.
25. McGehee, John R., "A Preliminary Experimental Investigation of an Energy-Absorption Process Employing Frangible Metal Tubing," NASA TN D-1477, October 1962.
26. McGehee, John R., "Experimental Investigation of Parameters and Materials for Fragmenting-Tube Energy-Absorption Process," NASA TN D-3268, February 1966.
27. Daigle, D. L. and Lonborg, J. O., "Evaluation of Certain Crushable Materials," Tech. Rpt. No. 32-120 (Contract No. NASw-6), Jet Propulsion Lab., C.I.T., January 15, 1961.
28. Lipson, S., "Cellular Aluminum for Use in Energy Dissipation Systems," NASA CR-95, 1964.
29. Baker, W. E., "Approximate Techniques for Plastic Deformation of Structures under Impulsive Loading," Shock and Vibration Digest, Vol. 7, No. 7, pp. 107-117, 1975.
30. Jones, N., "A Literature Review of the Dynamic Plastic Response of Structures," Shock and Vibration Digest, Vol. 7, No. 8, pp. 88-105, 1975.
31. Goldsmith, W., Impact, Arnold, 1960.
32. Rawlings, B., "Recent Progress in the Study of Steel Structures Submitted to Impulsive Overload," Dynamic Waves in Civil Engineering, (eds.) D. A. Howells, I. P. Haigh and C. Taylor, Wiley Interscience, pp. 543-565, 1971.
33. Symonds, P. S., "Survey of Methods of Analysis of Plastic Deformation of Structures Under Dynamic Loadings," Brown University, Rept. BU/NSRDC/1-67, 1967.
34. Johnson, W., Impact Strength of Materials, Arnold, London and Crane Russak, (U.S.), 1972.
35. Jones, N., Dumas, J. W., Giannotti, J. G., and Grassit, K. E., "The Dynamic Plastic Behavior of Shells," Dynamic Response of Structures, (eds.), G. Herrmann and N. Perrone, Pergamon Press, pp. 1-29, 1972.

36. Lee, L. H. N., "Dynamic Plasticity," *Hud. Engr. Des.* 27, pp. 386-397, 1974.
37. Krajcinovic, D., "Dynamic Response of Rigid-Ideally Plastic Structures," *Shock and Vibration Digest*, Vol. 5, No. 2, pp. 1-8, February 1973.
38. Witmer, E. A., Balmer, H. A., Leech, J. W., and Pian T. H. H., "Large Dynamic Deformations of Beams, Rings, Plates, and Shells," *AIAA Jnl.*, Vol. 1, No. 8, pp. 1848-1857, 1963.
39. Leech, J. W., Witmer, E. A., and Pian, T. H. H., "Numerical Calculation Techniques for Large Elastic-Plastic Transient Deformations of Thin Shells," *AIAA Jnl.* Vol. 6, No. 12, pp. 2352-2359, 1968.
40. Morino, L., Leech, J. W., and Witmer, E. A., "An Improved Numerical Calculation Technique for Large Elastic-Plastic Transient Deformations of Thin Shells, Parts 1 and 2," *J. of Appl. Mech.*, Vol. 38, No. 2, pp. 423-436, 1971.
41. Wu, R. W. H. and Witmer, E. A., "Finite Element Analysis of Large Elastic-Plastic Transient Deformations of Simple Structures," *AIAA Jnl.*, Vol. 9, No. 9, pp. 1719-1724, 1971
42. Wu, R. W. H. and Witmer, E. A., "Nonlinear Transient Responses of Structures by the Spatial Finite-Element Method," *AIAA Jnl.* Vol. 11, No. 8, pp. 1110-1117, 1973.
43. Vogel, W. H., Rangaiah, V. P. and Neubert, V. H., "Shock Analysis of Structural Systems," Contract No. Nonr-(58(28) (X), Interim Report No. 9, 1970.
44. Brown, W. G., "Dynamic Properties of Beams of Cold-Rolled Steel," M. S. Thesis, The Pennsylvania State University, 1967.
45. Frick, T. M. and Neubert, V. H., "Viscoplastic Bending of Copper-Nickel and Steel Tubing," *Jnl. of Eng'g. Materials and Technology*, Vol. 99, pp 387-392, October, 1977.
46. Butt, Lowell T., R. D. Short, Jr., and E. A. Thornton, "Shock Damage Mechanisms of a Simple Structure," Report No. 2191, Structural Mechanics Laboratory, Underwater Research Division, Portsmouth, VA., March, 1967.
47. Butt, Lowell T., "Shock Damage Analysis of a Three-Span Beam," Report 5259, Structures Department, Underwater Explosions Research Division, Portsmouth, VA., August 1972.
48. Burns, A. B., Guide for the Selection & Application of Shock Mounts for Shipboard Equipment, Contract No. Nobs-78963, Bu Ships Code 423, September 1, 1961.
49. Jones, N., "On the Collision Protection of Ships," *Nuclear Engineering and Design*, Vol. 38, pp. 229-240, 1976.
50. Perrone, N., "Crashworthiness and Biomechanics of Vehicle Impact," in Dynamic Response of Biomechanical Systems, ASME, New York, N. Y., 1970.
51. Yim, S. J., "Large Deflection Response of Elastic/Viscoplastic Beams under Combined Tension and Bending," Doctoral Thesis, The Pennsylvania State University, November, 1978 (contains extensive Supplemental Bibliography).

DISTRIBUTION LIST

DEPARTMENT OF DEFENSE

Assistant to the Secretary of Defense
Atomic Energy
ATTN: Executive Assistant

Defense Advanced Rsch. Proj. Agency
ATTN: TIO

Defense Technical Information Center
12 cy ATTN: DD

Defense Intelligence Agency
ATTN: DB-4C
ATTN: RDS-3A

Defense Nuclear Agency
ATTN: DDST
2 cy ATTN: SPSS
4 cy ATTN: TITL

Field Command
Defense Nuclear Agency
ATTN: FCPR

Field Command
Defense Nuclear Agency
Livermore Division
ATTN: FCPRL

Interservice Nuclear Weapons School
ATTN: TTV

Undersecretary of Def. for Rsch. & Engrg.
ATTN: Strategic & Space Systems (OS)

DEPARTMENT OF THE ARMY

Deputy Chief of Staff for Rsch. Dev. & Acq.
Department of the Army
ATTN: DAMA-CSS-N

Harry Diamond Laboratories
Department of the Army
ATTN: DELHD-I-TL
ATTN: DELHD-N-P

U.S. Army Ballistic Research Labs.
ATTN: DRDAR-TSB-S

U.S. Army Engr. Waterways Exper. Station
ATTN: Library

U. S. Army Material & Mechanics Rsch. Ctr.
ATTN: DRXMR-TE, R. Shea

DEPARTMENT OF THE NAVY

Naval Construction Battalion Center
ATTN: Code LO8A, Library

Naval Electronic Systems Command
ATTN: PME 117-21

DEPARTMENT OF THE NAVY (Continued)

David Taylor Naval Ship R & D Center
ATTN: Code 172
ATTN: Code 2740
ATTN: Code 174
ATTN: Code 173
ATTN: Code 1740.4
ATTN: Code 1740.1
ATTN: Code L42-3
2 cy ATTN: Code 1770.1

Naval Facilities Engineering Command
ATTN: Code 09M22C

Naval Ocean Systems Center
ATTN: Code 4471

Naval Postgraduate School
ATTN: Code 0142
ATTN: Code 69NE

Naval Research Laboratory
ATTN: Code 8406
ATTN: Code 2627
ATTN: Code 8100
ATTN: Code 8440
ATTN: Code 8445
ATTN: Code 6380
ATTN: Code 8301
ATTN: Code 8003

Naval Sea Systems Command
2 cy ATTN: SEA-08
2 cy ATTN: SEA-323
2 cy ATTN: SEA-3221
ATTN: SEA-09G53

Naval Surface Weapons Center
ATTN: Code R15
ATTN: Code R10
ATTN: Code R13
ATTN: Code F31
2 cy ATTN: Code R14

Naval Surface Weapons Center
ATTN: Technical Library & Info. Svs. Br.

Naval Weapons Center
ATTN: Code 233, Technical Library

Naval Underwater Systems Center
ATTN: Code 401, J. Kalinowski
ATTN: Code 401, J. Patel

Naval Underwater Systems Center
ATTN: Code 363, P. Paranzino
ATTN: Code EM

Office of Naval Research
ATTN: Code 715
4 cy ATTN: Code 474, N. Perrone

DEPARTMENT OF THE NAVY (Continued)

Office of the Chief of Naval Operations

ATTN: OP 982
ATTN: OP 951
ATTN: OP 981N1
ATTN: OP 21
ATTN: OP 604C

Strategic Systems Project Office
Department of the Navy
ATTN: NSP-43

DEPARTMENT OF THE AIR FORCE

Air Force Institute of Technology
ATTN: Library

Air Force Weapons Laboratory
Air Force Systems Command
ATTN: SUL

DEPARTMENT OF ENERGY CONTRACTORS

Lawrence Livermore Laboratory
ATTN: Document Control for Technical
Information Dept. Library

Los Alamos Scientific Laboratory
ATTN: Document Control for D. Nowlin
ATTN: Document Control for MS 364,
Class. Reports Library

Sandia Laboratories
ATTN: Document Control for 3141

Sandia Laboratories
Livermore Laboratory
ATTN: Document Control for Library &
Security Classification Div.

DEPARTMENT OF DEFENSE CONTRACTORS

Bolt Beranek & Newman, Inc.
ATTN: R. Haberman

Cambridge Acoustical Assoc., Inc
ATTN: M. Junger

Columbia University
ATTN: H. Bleich
ATTN: F. Dimaggio

General Dynamics Corp.
2 cy ATTN: M. Pakstys

DEPARTMENT OF DEFENSE CONTRACTORS (Continued)

Kaman Avidyne
ATTN: Library

Kaman Sciences Corp.
ATTN: Library

Lockheed Missiles and Space Co., Inc.
ATTN: Technical Information Center
ATTN: T. Geers

Merritt CASES, Inc.
ATTN: Library

Pacifica Technology
ATTN: J. Kent

Patel Enterprises, Inc.
ATTN: M. Patel

University of Pennsylvania
10 cy ATTN: V. Neubert
ATTN: S. Yim

R & D Associates
ATTN: Technical Information Center
ATTN: C. MacDonald

SRI International
ATTN: G. Abrahamson
ATTN: A. Florence

Tetra Tech, Inc.
ATTN: Library

Weidlinger Assoc., Consulting Engineers
2 cy ATTN: M. Baron

Weidlinger Assoc., Consulting Engineers
ATTN: J. Isenberg

Physics Applications, Inc.
ATTN: C. Vincent

General Electric Company-TEMPO
ATTN: DASIAC

University of Illinois
ATTN: N. Newmark

Institute for Defense Analyses
ATTN: Classified Library